

Arterial and Atherosclerotic Plaque Biomechanics with Application to Stent Angioplasty Modeling

Brían L. O'Reilly, Claire Conway, J. Patrick McGarry
and Peter E. McHugh

Abstract This chapter provides a brief review of continuum mechanics in relation to application in vascular biomechanics. The initial focus is on arterial tissue, where fundamental constitutive representations, tissue anisotropy, tissue remodeling and damage modeling are overviewed. The focus then shifts to diseased tissue (atherosclerotic plaque tissue), where experimental mechanical characterization, and constitutive and damage modeling are reviewed. Conclusions are drawn on what has been achieved thus far, and the main challenges for the future in characterizing and modeling this complex tissue are identified. Finally, the application of the arterial mechanics in the computational modeling of the stent angioplasty procedure is considered, with future challenges identified.

1 Introduction

Mathematical modeling, both analytical and computational, is a vitally important component of soft tissue biomechanics. In the case of vascular biomechanics, as is of interest here, modeling can generate deep insight into the fundamental physical and mechanical behavior of the tissue, in both healthy and diseased states. In addition, modeling is vitally important for the analysis, design, and performance assessment of devices and implants used in surgical interventions of the vasculature. Of particular interest here is the stent angioplasty procedure, for the treatment of atherosclerosis, where a stent is introduced into the blocked region of a diseased artery and expanded to restore arterial lumen patency. All proper modeling investigations, not least in the present case of vascular biomechanics, are built on the generation and availability of accurate experimental data, for model development, calibration, and validation. This chapter summarises some of the most important mathematical modeling work performed in the vascular biomechanics domain over the past 20 years or so, focusing

B.L. O'Reilly · C. Conway · J.P. McGarry · P.E. McHugh (✉)
National University of Ireland, Galway, Ireland
e-mail: peter.mchugh@nuigalway.ie

© Springer International Publishing Switzerland 2017
G.A. Holzapfel and R.W. Ogden (eds.), *Biomechanics: Trends in Modeling and Simulation*, Studies in Mechanobiology, Tissue Engineering and Biomaterials 20, DOI 10.1007/978-3-319-41475-1_5

on approaches that can be implemented computationally using the finite element method. Particular attention is paid to reviewing modeling work on diseased tissue.

The chapter starts with a brief review of the aspects of continuum mechanics that are most relevant to vascular biomechanics. The focus is then applied to arterial tissue, where fundamental constitutive representations, tissue anisotropy, tissue remodeling, and damage modeling are overviewed. The focus then shifts to diseased tissue (atherosclerotic plaque tissue), where experimental mechanical characterization, and constitutive and damage modeling are reviewed. Conclusions are drawn on what has been achieved thus far, and the main challenges for the future in characterizing and modeling this complex tissue are identified.

In the final section of the chapter, focus is applied to the computational modeling of stent angioplasty, where many of the modeling features described in the previous sections are implemented. The work reviewed in this section illustrates the practicalities of attempting to achieve an accurate numerical simulation of stent deployment, and points up challenges still to be overcome in relation to such modeling efforts. Finally, the reviewed work is used to generate recommendations for the improvement of regulatory body guidelines for the computational modeling of stent angioplasty as part of the medical device regulatory approval process.

2 Finite Deformation Kinematics: Strain and Stress Measures

Standard tensor and indicial notation is used throughout the following, and tensor/vector components are written with respect to the standard orthonormal base vectors \mathbf{e}_1 , \mathbf{e}_2 , and \mathbf{e}_3 . The right and left Cauchy–Green tensors are given below, respectively, where \mathbf{F} is the deformation gradient tensor

$$\mathbf{C} = \mathbf{F}^T \mathbf{F}, \quad \mathbf{B} = \mathbf{F} \mathbf{F}^T. \quad (1)$$

Hyperelasticity is a type of constitutive model characterized by the strain-energy density function W , which can be written as a function of \mathbf{F} . The gradient of the strain-energy density with respect to \mathbf{F} yields the nominal stress \mathbf{S}

$$\mathbf{S} = \frac{\partial W(\mathbf{F})}{\partial \mathbf{F}}. \quad (2)$$

The Cauchy (true) stress, $\boldsymbol{\sigma}$, is defined as the force over the area in the current configuration, and is given by the following, where J is the Jacobian of the deformation (determinant of \mathbf{F}),

$$\boldsymbol{\sigma} = \frac{1}{J} \mathbf{F} \frac{\partial W(\mathbf{F})}{\partial \mathbf{F}}, \quad J = |\mathbf{F}|. \quad (3)$$

In isotropic materials, W can be written in terms of the eigenvalues of \mathbf{C} . These eigenvalues are the squares of the principal stretches, λ_1 , λ_2 , and λ_3 , shown below

$$[\mathbf{C}] = \begin{bmatrix} \lambda_1^2 & 0 & 0 \\ 0 & \lambda_2^2 & 0 \\ 0 & 0 & \lambda_3^2 \end{bmatrix}. \quad (4)$$

Invariants of the strain can be defined to eliminate coordinate axes dependence in the constitutive expressions

$$I_1 = \lambda_1^2 + \lambda_2^2 + \lambda_3^2, \quad I_2 = \lambda_2^2 \lambda_3^2 + \lambda_3^2 \lambda_1^2 + \lambda_1^2 \lambda_2^2, \quad I_3 = \lambda_1^2 \lambda_2^2 \lambda_3^2. \quad (5)$$

The Jacobian determines volume change in a material and can be related to the third invariant as follows:

$$J = \sqrt{I_3}. \quad (6)$$

Using these relationships allows the Cauchy stress to be written in terms of the invariants, with implied summation over the three invariant indices $i = 1, 2, 3$

$$\boldsymbol{\sigma} = \frac{1}{J} \mathbf{F} \frac{\partial W(\mathbf{F})}{\partial \mathbf{F}} = \frac{1}{J} \mathbf{F} \left(\frac{\partial W}{\partial I_i} \frac{\partial I_i}{\partial \mathbf{F}} \right). \quad (7)$$

This leads to the general result for an isotropic hyperelastic material

$$\boldsymbol{\sigma} = \frac{2}{J} \left(\frac{\partial W}{\partial I_1} + I_1 \frac{\partial W}{\partial I_2} \right) \mathbf{B} - \frac{2}{J} \frac{\partial W}{\partial I_2} \mathbf{B}^2 + 2J \frac{\partial W}{\partial I_3} \mathbf{I}. \quad (8)$$

3 Arterial Tissue

3.1 Fundamental Representation

Arterial tissue has been extensively linked in studies with the characteristics of hyperelasticity. Significant focus has been applied to the representation of tissue anisotropy; models have been developed to capture the anisotropy that occurs due to the directionality of the collagen and elastin fibers in the different layers of the artery.

Arterial tissue consists of layers, where each layer makes a different contribution to the collective mechanical properties of the tissue, with each layer having its own fiber orientation characteristics. In the adventitial layer, for example, are helically distributed collagen fibers. The layered structure and the corresponding fiber orientations are illustrated in Fig. 1. The most popular constitutive model implemented in recent studies of arterial mechanics is the now commonly referred to as the Holzapfel–Gasser–Ogden (HGO) model, first presented by Holzapfel et al. (2000), and further

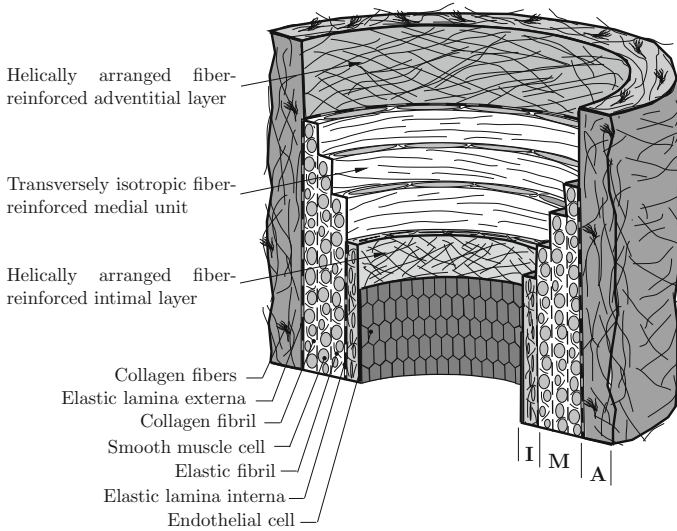


Fig. 1 Representative image of the cross-section along an arterial displaying the layers and collagen fiber orientations within the wall (Gasser et al. 2006). Reproduced with permission

elucidated in a series of papers, including Gasser et al. (2006). This model assumes material incompressibility and introduces a unit vector \mathbf{M} in order to define the orientation of a family of transversely isotropic aligned collagen fibers in the arterial tissue, and a related strain invariant I_4 , which represents the square of the stretch in the fiber direction, through the following

$$I_4 = \mathbf{M} \cdot (\mathbf{C}\mathbf{M}) = M_i C_{ij} M_j, \quad \mathbf{m} = \mathbf{F}\mathbf{M}, \quad m_i = F_{ij} M_j. \quad (9)$$

An illustration of the fiber angle γ is given in Fig. 2.

In the context of incompressibility in the material $J = 1$ and the general expression for the stress can be written as follows:

$$\boldsymbol{\sigma} = -p\mathbf{I} + 2 \left(\frac{\partial W}{\partial I_1} + I_1 \frac{\partial W}{\partial I_2} \right) \mathbf{B} - 2 \frac{\partial W}{\partial I_2} \mathbf{B}^2, \quad (10)$$

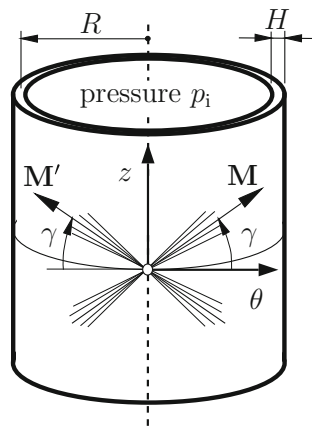
where p is a Lagrange multiplier that can be interpreted as a hydrostatic pressure.

For the present consideration of the HGO model it is useful to introduce isochoric (deviatoric) counterparts of the deformation gradient, deformation tensors, and invariants

$$\mathbf{F} = (J^{1/3} \mathbf{I}) \bar{\mathbf{F}}, \quad \bar{\mathbf{C}} = \bar{\mathbf{F}}^T \bar{\mathbf{F}}, \quad \bar{\mathbf{B}} = \bar{\mathbf{F}} \bar{\mathbf{F}}^T, \quad (11)$$

$$\bar{I}_1 = J^{-2/3} I_1, \quad \bar{I}_4 = J^{-2/3} I_4. \quad (12)$$

Fig. 2 Representative image of the cross-section along an artery displaying the layers and collagen fiber orientations within the wall. γ is the angle between the fiber directions \mathbf{M} and \mathbf{M}' and the circumferential direction. Adapted from Gasser et al. (2006). Reproduced with permission



The original quantities and their isochoric counterparts are equal for the incompressible case, hence the isochoric quantities are used in the following for overall consistency.

\bar{I}_4 can be utilized to split the energy density function into a term describing the isotropic deformation of the ground substance (tissue matrix) and a second term describing the anisotropic deformation of the transversely isotropic family of aligned fibers, through the following equation

$$W = W_g(\bar{I}_1) + W_f(\bar{I}_4), \quad (13)$$

which can be more comprehensively expressed as

$$W_g(\bar{I}_1) = \frac{1}{2}\mu(\bar{I}_1 - 3), \quad W_f(\bar{I}_4) = \frac{k_1}{k_2}\{\exp[k_2(\bar{I}_4 - 1)^2] - 1\}. \quad (14)$$

The coefficients are as follows: μ is the shear modulus, k_1 is a stress-like parameter, and k_2 is a dimensionless parameter.

The exponential function in the strain-energy function captures the strong stiffening effects of the interior tensions in collagen fibers at higher strain levels. Using these expressions the relationship for the Cauchy stress is defined as

$$\boldsymbol{\sigma} = -p\mathbf{I} + \mu\mathbf{B} + 4k_1(\bar{I}_4 - 1)\exp[k_2(\bar{I}_4 - 1)^2]\bar{\mathbf{m}} \otimes \bar{\mathbf{m}}, \quad \bar{\mathbf{m}} = \bar{\mathbf{F}}\mathbf{M}. \quad (15)$$

Extending this framework to better represent arterial tissue structure is the inclusion of a second fiber family which is transversely symmetrical to the first fiber family (see Fig. 2), and identified by the unit vector \mathbf{M}' . For completeness, the two families are described below using the invariants \bar{I}_4 and \bar{I}_6

$$\bar{I}_4 = \mathbf{M} \cdot (\bar{\mathbf{C}}\mathbf{M}), \quad \bar{I}_6 = \mathbf{M}' \cdot (\bar{\mathbf{C}}\mathbf{M}'). \quad (16)$$

The strain-energy density can now be written as

$$W = W_g(\bar{I}_1) + W_f(\bar{I}_4, \bar{I}_6), \quad (17)$$

$$W_f(\bar{I}_4, \bar{I}_6) = \frac{k_1}{2k_2} \sum_{i=4,6} \{\exp[k_2(\bar{I}_i - 1)^2] - 1\}, \quad (18)$$

with $W_g(\bar{I}_1)$ given by (14)₁, and thus

$$\begin{aligned} \boldsymbol{\sigma} = & -p\mathbf{I} + \mu\mathbf{B} + 2k_1(\bar{I}_4 - 1) \exp[k_2(\bar{I}_4 - 1)^2] \bar{\mathbf{m}} \otimes \bar{\mathbf{m}} \\ & + 2k_1(\bar{I}_6 - 1) \exp[k_2(\bar{I}_6 - 1)^2] \bar{\mathbf{m}}' \otimes \bar{\mathbf{m}}', \end{aligned} \quad (19)$$

with $\bar{\mathbf{m}}' = \bar{\mathbf{F}}\mathbf{M}'$ and $\bar{\mathbf{m}}$ defined in (15)₂.

Going further, consider that, anatomically, individual fibers in a fiber family are not aligned, but are distributed around a mean direction (see Fig. 2). In the HGO model, this can be captured by introducing a generalized structure tensor \mathbf{H} to account for the dispersion around the mean \mathbf{M} and \mathbf{M}' vectors in the arterial tissue, written for the \mathbf{M} case as follows:

$$\mathbf{H} = \kappa\mathbf{I} + (1 - 3\kappa)\mathbf{M} \otimes \mathbf{M}, \quad \kappa = \frac{1}{4} \int_0^\pi \rho \sin^3 \Theta \, d\Theta, \quad (20)$$

where κ is a dispersion parameter and ρ is an orientation density function based on a π periodic von Mises distribution of fibers rotationally symmetric around \mathbf{M} . A graphical representation of this function is given in Fig. 3, while a three-dimensional representation is provided in Fig. 4.

\bar{I}_4 must then be modified to account for dispersion and is replaced with \bar{I}_4^* , defined as follows:

$$\bar{I}_4^* = \mathbf{H} : \bar{\mathbf{C}} = H_{ij} \bar{C}_{ij}, \quad (21)$$

which can also be simplified to the following:

$$\bar{I}_4^* = \kappa \bar{I}_1 + (1 - 3\kappa) \bar{I}_4. \quad (22)$$

This leads to the following expression for W_f

$$W_f(\bar{I}_1, \bar{I}_4) = \frac{k_1}{k_2} \{\exp[k_2(\bar{I}_4^* - 1)^2] - 1\} = \frac{k_1}{k_2} \{\exp[k_2(\kappa \bar{I}_1 + (1 - 3\kappa) \bar{I}_4 - 1)^2] - 1\}. \quad (23)$$

Repeating the process for \mathbf{M}' yields

$$\mathbf{H}' = \kappa\mathbf{I} + (1 - 3\kappa)\mathbf{M}' \otimes \mathbf{M}', \quad \bar{I}_6^* = \kappa \bar{I}_1 + (1 - 3\kappa) \bar{I}_6. \quad (24)$$

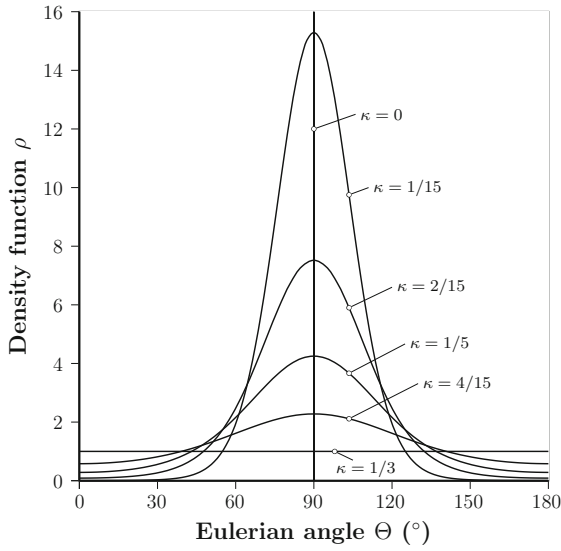


Fig. 3 A two-dimensional graphical representation of the (transversely isotropic) von Mises distribution of collagen fibers (Gasser et al. 2006). Reproduced with permission

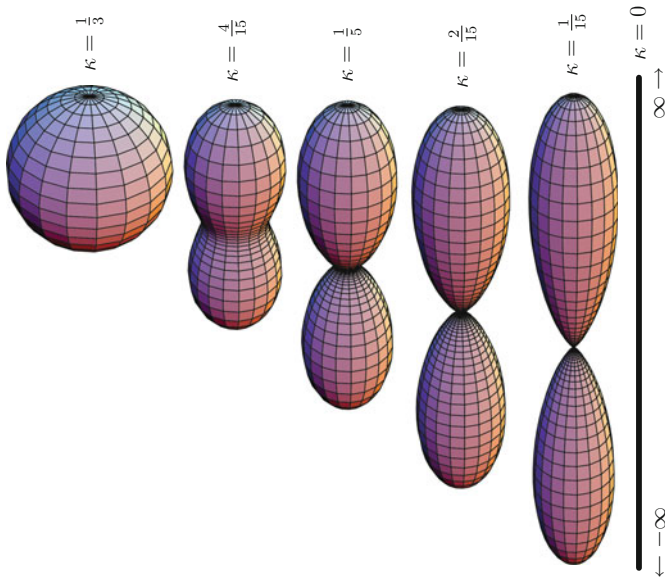


Fig. 4 A three-dimensional graphical representation of the (transversely isotropic) von Mises distribution of collagen fibers (Gasser et al. 2006). Reproduced with permission

and then finally

$$W = W_g(\bar{I}_1) + W_f(\bar{I}_1, \bar{I}_4, \bar{I}_6), \quad (25)$$

where

$$W_f(\bar{I}_1, \bar{I}_4, \bar{I}_6) = \frac{k_1}{2k_2} \sum_{i=4,6} \{\exp[k_2(\bar{I}_i^* - 1)^2] - 1\} \quad (26)$$

and $W_g(\bar{I}_1)$ is again given by (14)₁.

Figure 5 shows the analytical solution to the HGO model for the case of a thin-walled tube, showing the influence of the mean alignment and dispersion coefficient on the overall mechanical properties. From the figure it can be seen that higher fiber dispersion κ correlates with lower fiber family orientation angle dependence γ .

For the case of compressible or slightly compressible materials, a recent study by Nolan et al. (2014) has demonstrated that the full forms of the anisotropic invariants (I_4, I_6) must be used. If the isochoric forms of the anisotropic invariants (\bar{I}_4, \bar{I}_6) are used when material volume change is permitted ($J \neq 1$) then significant errors in the computed stress can emerge. An experimental study on ovine aortic tissue by Nolan and McGarry (2015) reveals significant material volume change and suggests that such tissue is compressible at a macroscopic continuum level. To fully characterize such phenomena, there is a need for further experimentation to be performed on muscular arterial tissue, including compressibility tests on healthy and diseased human arterial tissue.

Two other phenomena that are important in the modeling of arterial tissue and that have been addressed in the literature are remodeling and damage.

3.2 Remodeling

Remodeling of fiber directions in arterial layers has been considered by a number of authors in the field of biomechanics. These studies typically assume that the mechanical stimuli (stress or strain) on arterial tissue determine the local fiber orientations, for example:

- Fibers will reorient towards the plane of maximum and intermediate principal directions of the tensorial stimuli.
- In this plane, the angle of fiber alignment with respect to maximum principal stimulus is determined by magnitudes of two maximum principal stimuli. In the principal stress case, where γ is angle of fiber alignment with respect to the maximum principal stress, and σ_1 and σ_2 are the maximum and intermediate principal stresses, $\tan \gamma$ can be written as a function, M , of the principal stress ratio:

$$\tan \gamma = M(\sigma_2/\sigma_1). \quad (27)$$

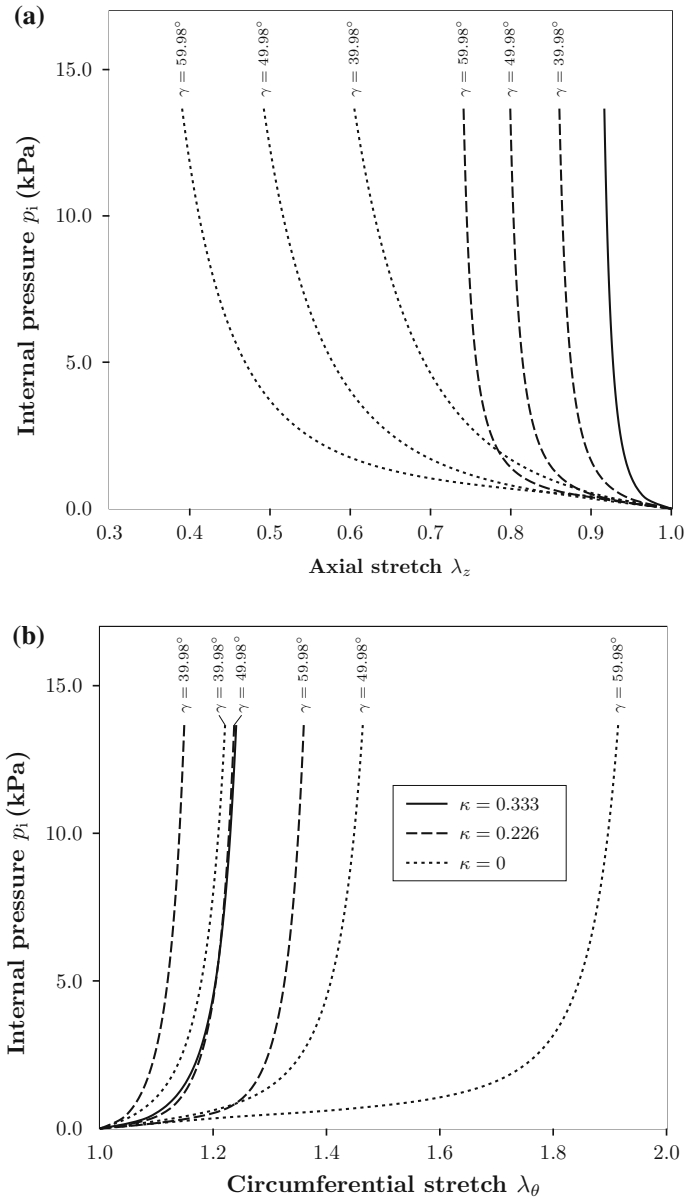


Fig. 5 Graphs depicting the influence of the mean fiber alignment and dispersion on the pressure response of the artery wall (Gasser et al. 2006). Reproduced with permission

Other approaches to the fiber remodeling have been discussed in more recent studies. Driessen et al. (2004) developed principal stress-based approaches for fiber remodeling using the principle discussed for dispersed fiber populations. Hariton et al. (2007) proposed a stress-based approach using the Holzapfel-type fibrous hyperelastic model discussed above (HGO without dispersion), where

$$\tan \gamma = M(\sigma_2/\sigma_1) = \sigma_2/\sigma_1. \quad (28)$$

Creane (2011) reviewed the topic of fiber remodeling and has developed a strain-based remodeling algorithm for dispersed fiber populations, based on the HGO model. This model uses an iterative method to create an optimal structure tensor for the fiber orientation for each fiber family (Creane 2011; Creane et al. 2012).

3.3 *Damage-Induced Softening*

Damage models are used to replicate the effects of stress softening in soft tissues. These types of models are needed to account for damage induced in soft tissues during supra-physiological loading, e.g., stenting procedure. This type of modeling uses a continuum approach and is distinct from microstructure and material separation modeling.

Most commonly, damage is modeled using a damage parameter, introduced into finite-deformation elasticity laws, to account for tissue softening in terms of a reduction in the mechanical properties and stress, which represents damage to collagen fibers and matrix in the tissue. A comprehensive review of this topic is given in Conway (2013). Analysis of this type can be classified under two major headings: continuum damage mechanics approach and pseudo-elasticity approach (Weisbecker et al. 2011).

3.3.1 **Continuum Damage Mechanics Approach**

A general form for a modified strain-energy density function, to account for damage, is given as (Miehe 1995)

$$W(\mathbf{C}, D) = (1 - D)W_0(\mathbf{C}), \quad (29)$$

where D is the damage parameter and W_0 is the undamaged strain-energy density function. There are two sub-categories to consider: discontinuous damage and continuous damage, as reviewed in Miehe (1995) and Peña and Doblaré (2009).

Discontinuous Damage

This form of damage is calculated by the accumulation of damage in the first loading cycle of a strain-controlled loading. In any subsequent load cycle, further damage may only be accumulated with strain energy exceeding the previous maximum strain energy achieved.

This is best described by the relationship below, where damage is governed by the quantity α , which represents the maximum undamaged strain-energy density achieved during the loading history (time: $0 \rightarrow t$) (Miehe 1995):

$$\alpha = \max W_0(\mathbf{C}(s)), \quad s \in (0, t). \quad (30)$$

During a typical loading history, involving loading, unloading, reloading, etc., there is no (further) damage accumulation when $W_0(\mathbf{C}) < \alpha$.

Continuous Damage

When determining this type of damage, the entire loading history is accounted for, and this type of damage can account for the continuous softening of a material over its lifespan. Damage is possible during loading in cycles of the same amplitude. The variable β is used to govern the continuous damage and monotonically increases with deformation through the following (Miehe 1995):

$$\beta = \int_0^t |\dot{W}_0(\mathbf{C}(s))| ds. \quad (31)$$

Comparison

Both discontinuous and continuous damage models are usually applied to only the isochoric (deviatoric) part of the deformation gradient tensor. In algebraic form, $W_0^{\text{ich}}(\mathbf{C})$.

The discontinuous model approach has been the more commonly applied of the two, arguably due to it being more physically relevant for soft tissues. For example, the well-known Mullins effect is well described by this model type; capturing this behavior is important because soft tissue loading and unloading curves have been observed to clearly exhibit the Mullins effect, as reviewed in Conway (2013). Studies that have used the soft tissue discontinuous modeling approach include: Hokanson and Yazdani (1997), Balzani et al. (2004, 2006, 2012), Rodríguez et al. (2006), Calvo et al. (2007), Alastrué et al. (2007), Brinkhues et al. (2009), Maher et al. (2011, 2012), Peña (2011).

Continuous damage modeling exhibits advantages in relation to the modeling of cyclic loading, for example, in relation to capturing hysteresis in arterial tissue cyclic stress-strain curves, and in relation to simulating the effects of preconditioning

loading histories performed prior to the testing proper. Studies in this domain include: Miehe (1995), Ehret and Itskov (2009), Peña and Doblaré (2009), Martin and Sun (2013).

Very good predictive performance for cyclic loading has been achieved using discontinuous and continuous modeling combinations, for example in: Miehe (1995), Peña et al. (2009), Martin and Sun (2013). Figure 3 from Peña et al. (2009) compares combined discontinuous and continuous model predictions for aortic tissue response under cyclic loading (Fig. 6a) with predictions for a discontinuous only (Fig. 6b) and a continuous only (Fig. 6c). The superior performance of the combined model is evident in this case.

Continuum damage mechanics approaches have been developed and applied to soft tissue in a range of contexts; in anisotropic tissue models to represent matrix and fiber damage, to capture material rate dependence and permanent deformation on unloading, and in models that include arterial tissue residual stresses. Example studies include: Hokanson and Yazdani (1997), Volokh (2008) (isotropic damage models); Balzani et al. (2004, 2006, 2012), Brinkhues et al. (2009), Gasser (2011) (collagenous damage models); Calvo et al. (2007), Rodríguez et al. (2008), Gracia et al. (2009), Peña et al. (2009), Weisbecker et al. (2011) (matrix and fiber damage models); Peña (2011) (rate dependent material damage); Maher et al. (2011) (inelastic isotropic damage).

3.3.2 Pseudo-Elasticity Approach

The pseudo-elasticity approach is another discontinuous damage modeling approach, but its formulation is not classified under the heading of continuum damage mechanics. In the pseudo-elasticity approach, if one considers strain controlled loading, then damage accumulates during the first loading path, with no damage accumulation on unloading, and in any subsequent load cycle there is no further damage unless the previous maximum strain energy is exceeded.

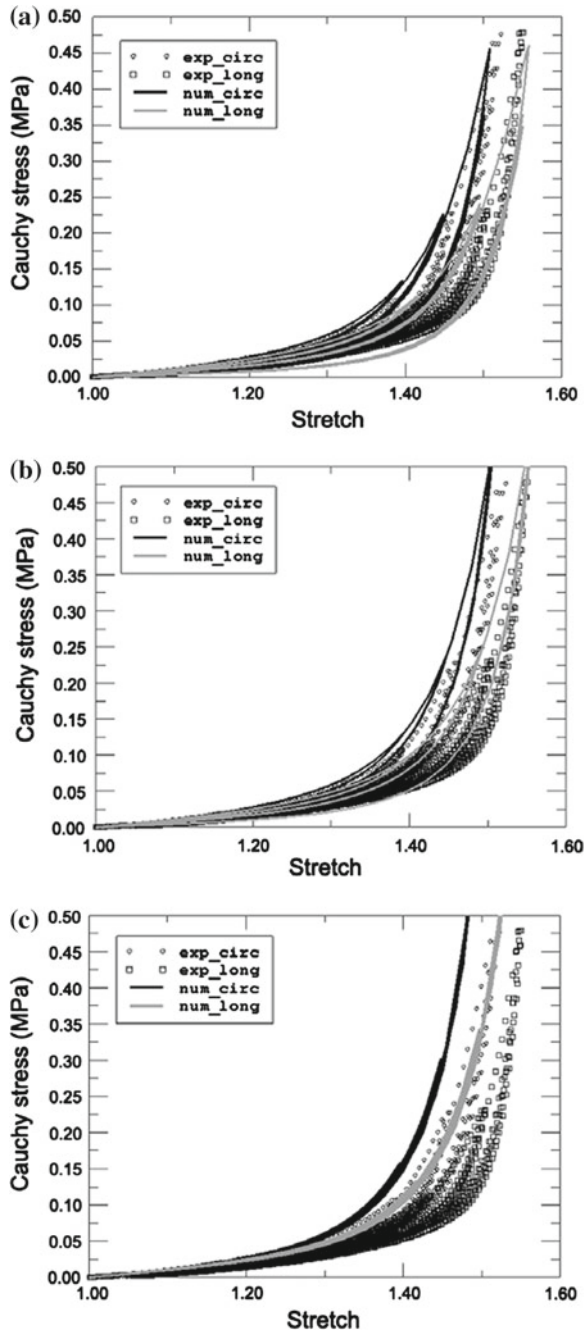
Ogden and Roxburgh (1999) developed a pseudo-elastic model that is widely used. This model was originally developed for modeling filled rubber elastomers that display the Mullins effect; this would later become the basis for the implementation of the Mullins effect in finite element software, i.e., Abaqus (2013).

The model can be described in terms of a modification of the strain-energy density to generate a pseudo-energy density

$$W(\mathbf{C}, \eta) = \eta W_0(\mathbf{C}) + \Phi(\eta), \quad (32)$$

where η is a damage parameter, W_0 is the undamaged strain-energy density and Φ is a damage function.

Fig. 6 Stress response of aortic tissue during cyclic biaxial tensile loading comparing experimental versus numerical models to capture damage. The different models used were mixed model (a), discontinuous model (b) and continuous (c) (from Peña et al. 2009). Reproduced with permission



Mullins Effect

The Mullins effect is important for arterial modeling as it is more physically relevant than pure hyperelasticity. The Mullins effect (see Fig. 7) is described by the loading and unloading curves following different loading paths, allowing for the formation of hysteresis loops in stress–strain curves during cyclic loading.

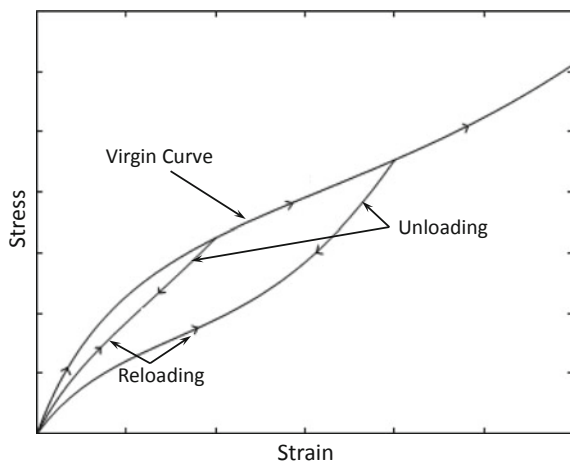
The Ogden and Roxburgh (1999) model assumes incompressibility. In simple tension, the stress is described by the following relationship, where λ is the principal stretch in the loading direction:

$$\sigma = \eta \lambda \frac{\partial W_0}{\partial \lambda}. \quad (33)$$

With reference to Fig. 7, on a virgin curve $\eta = 1$ and the loading follows the path $\sigma = \lambda \partial W_0 / \partial \lambda$. Upon unloading η becomes less than 1; there a softening effect and the material unloads along a lower stress path given by (33). As unloading progresses, the damage parameter reduces gradually to a minimum value $\eta = \eta_m < 1$ which, in turn, is determined by the original point of unload on the virgin curve. Upon reloading the material reloads along the softer curve with η gradually increasing, until the virgin curve is re-joined ($\eta = 1$), and further loading continues along the virgin curve. If a subsequent unloading event occurs, the process described above is repeated. An explicit form of η is given in Ogden and Roxburgh (1999) as follows, where r and m are model parameters, and W_0^m is the maximum value of the pseudo-energy function reached over the loading history:

$$\eta = 1 - \frac{1}{r} \operatorname{erf} \left[\frac{1}{m} (W_0^m - W_0) \right]. \quad (34)$$

Fig. 7 Stress/strain response of a material exhibiting an idealized Mullins effect. Adapted from Ogden and Roxburgh (1999). Reproduced with permission



The model is normally applied to the isochoric part of the deformation, but the framework can be extended to compressible materials.

Pseudo-elastic modeling approach developments include the representation of damage in anisotropic fibrous soft biological materials, better definitions of the hysteresis loops observed in cyclic loading and also the implementation of residual permanent deformation upon unloading. Example studies include: Ogden and Roxburgh (1999), Dorfmann and Ogden (2003, 2004), Franceschini et al. (2006), Ciarletta et al. (2008), Peña and Doblaré (2009), Peña et al. (2011), Weisbecker et al. (2012).

Important differences between the continuum damage mechanics and pseudo-elastic modeling approaches are that continuum damage mechanics allows for continuous and discontinuous softening, while pseudo-elastic model calibration from experimental data is typically easier since material parameters and damage model parameters can be fitted independently (Weisbecker et al. 2011).

4 Atherosclerotic Plaque

4.1 Introduction

Atherosclerotic plaque is an extremely complex structure with wide variations in both geometries and constituents. It is really a term for a wide range of geometries and structures that can change over time: soft lesions evolve to become hard calcified lesions. A schematic of the cross section of an atherosclerotic plaque is presented in Fig. 8. In this illustration, components such as lipid pools, calcifications and a fibrous cap are shown. In more advanced stages, stable lesions can continue to grow and also become highly calcified. Alternatively the fibrous caps can become unstable, leading to rupture and the formation of thrombus material, which can lead to embolism formation in the blood flow. A particularly dangerous situation is that of ‘vulnerable’ plaque, where the lesion can become unstable and the fibrous cap rupture early in lesion development; detection of early stage plaque vulnerability is still a major clinical challenge. For additional information on atherosclerosis please refer to Stary (1999).

The experimental characterization and modeling of plaque tissue is distinctly lacking in comparison to the extent of experimental characterization and modeling of healthy arterial tissue, and still represents a frontier for vascular mechanics and modeling. The importance of accuracy in the modeling of atherosclerotic plaque is paramount in the accurate prediction of the performance of vascular implants, such as vascular stents. Further to this, improvements in modeling capabilities for the prediction of implant performance could be very beneficial in the evolution of regulatory approval processes, for example, Food and Drug Administration (FDA 2010) requirements for the finite element modeling of stents as part of the medical device regulatory approval process.

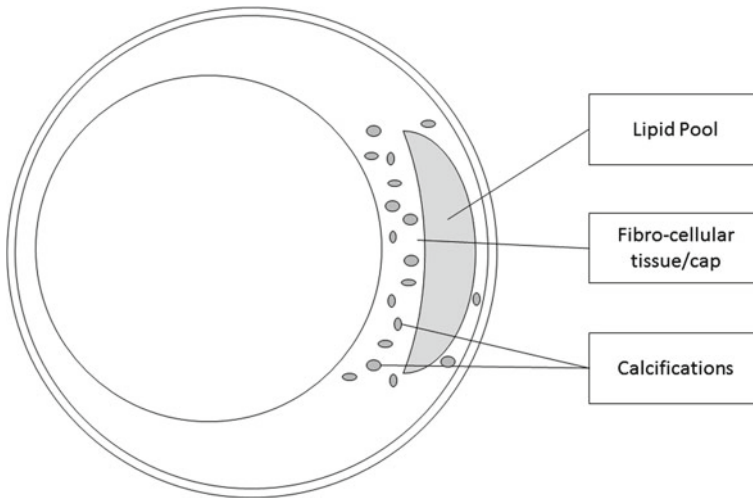


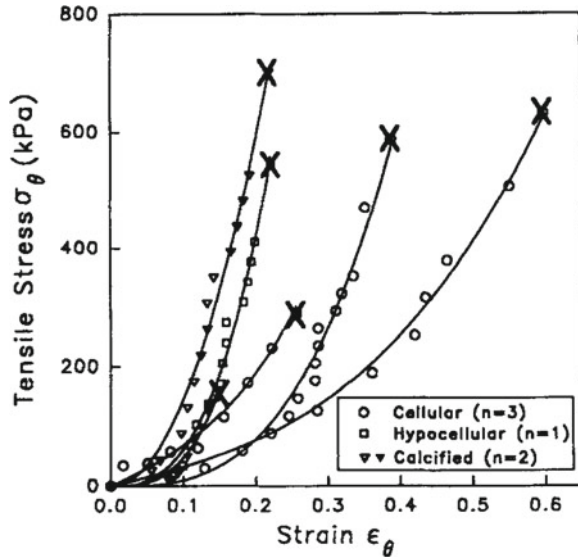
Fig. 8 Schematic of the cross section of an atherosclerotic plaque. Plaque constituents usually include lipid pools, a fibrous cap and calcifications

4.2 *Experimental Mechanical Characterization and Testing*

There are many challenges in the mechanical testing of atherosclerotic plaque tissue; it can be very soft and typically contains fluidic regions leading to issues in the handling and gripping of the tissue. There is difficulty in obtaining and isolating plaque tissue, and in particular for human tissue, for obvious reasons. Such difficulties present significant challenges in relation to trying to ensure material consistency for testing across different testing programmes and in relation to test reproducibility. The tissue is inherently highly heterogeneous and a broad range of structural variability exists, leading to a discussion of whether testing entire plaques or cut sections of a plaque is more appropriate. One major limitation to plaque tissue analysis, characterization and testing is the lack of a robust animal model of atherosclerotic plaque that is sufficiently representative of the disease in humans; the lack of such a model has significant implications for material availability, consistency and test reproducibility.

In the literature that is available, the main approach to experimental testing is macroscopic mechanical testing, focusing on compressive and tensile loading, and extracting overall mechanical response (stress–strain curves) and mechanical properties, including elastic modulus and ultimate strength (UTS), etc. Relatively speaking, there has been a limited focus on determining local/sub-structure tissue mechanical properties. Examples of studies focusing on macroscopic mechanical characterization include: Loree et al. (1994), Topoleski et al. (1997), Salunke et al. (2001), Walraevens et al. (2008), Maher et al. (2009, 2011), Teng et al. (2009), Lawlor et al. (2011), Mulvihill et al. (2013). Also reported in a number of these studies

Fig. 9 Data from Loree et al. (1994) tensile stress-strain curves for 6 fractured plaque specimens categorized by plaque type. Reproduced with permission



are macroscopic constitutive model fits to the experimental stress-strain data, using neo-Hookean and polynomial hyperelastic models for example.

The study of Loree et al. (1994) is an influential early study where the broad variation in mechanical response was clearly illustrated (see Fig. 9) as a function of plaque material type. Useful data on basic stress-strain curve shapes, and fracture stress and strain ranges, was reported; for example fracture stresses in the range 149–701 kPa, and strains in the range 15–60%, were reported. These data have been used as the basis for a number of plaque constitutive model calibrations in subsequent studies, including Gastaldi et al. (2010), Conway et al. (2012, 2014), Morlacchi et al. (2013). The more recent study of Maher et al. (2009) also illustrates significant tissue type dependence and also significant differences between tensile and compressive loading response (see Fig. 10).

One difficulty, due to the heterogeneity and broad range of structural variability, is that a definitive and standardized tissue type categorization has not been established, and the tissue type descriptions reported in different studies are very much study dependent, where the authors have made efforts to come to terms with the nature of the tissue samples available in any given instance. This adds a layer of complexity and uncertainty to the interpretation of mechanical property data that is not present for traditional materials, where constituents, manufacturing route and mechanical properties generally adhere to well established standards. The Loree et al. (1994) and Maher et al. (2009) studies illustrate this point for plaque (Figs. 9 and 10); ‘cellular’, ‘hypocellular’ and ‘cholucent’ tissue types are identified, but these are quite subjectively defined as determined by the specific tissue at hand and the specific microscopy/characterization method employed. In the same vein, a recent study by Barrett et al. (2016) has proposed a number of calcified plaque sub-classifications.

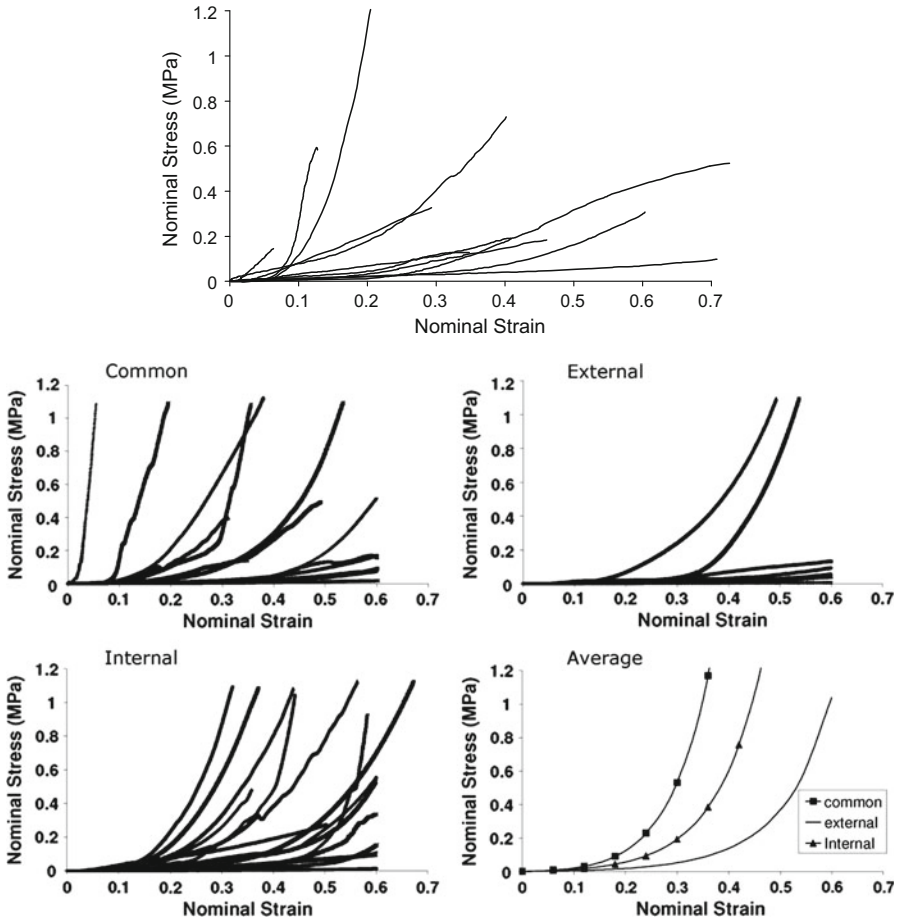


Fig. 10 Figures from Maher et al. (2009) for mechanical testing of carotid plaque: the upper figure shows tensile stress-strain response, and the group of four figures show compressive stress-strain response (unconfined compression), depending on tissue type. The average curves were obtained using a mean set of hyperelastic constants using a second order polynomial hyperelastic strain-energy function. Reproduced with permission

The relatively small number of studies focusing on plaque tissue sub-structure characterization includes those given in Table 1. A range of testing methods has been used, including tensile and compressive mechanical testing, rheometry and nano-indentation, to resolve the mechanical response and behavior of individual plaque constituents such as the fibrous cap, lipid core, calcifications, etc. Anisotropy of constituent layers in plaque has also been measured through tensile testing in axial and circumferential arterial directions (Holzapfel et al. 2004; Teng et al. 2009).

Nano- and micro-indentation presents very useful possibilities for determining constituents' mechanical behavior, since the necessity for extracting test samples of

Table 1 Experimental studies reporting on plaque tissue constituent mechanical characterization

Reference	Location	Method	Constituents	Data reported/model fit
Chai et al. (2013)	Carotid	Indentation	Fibrous cap	Reported: elastic moduli
			Intima	
			Lipid core	
Barrett et al. (2009)	Carotid	Indentation	Fibrous cap	Model fit: neo-Hookean
Ebenstein et al. (2009)	Carotid	Indentation	Calcification	Reported: reduced moduli
			Fibrous tissue	
			Hematoma (clot)	
Holzapfel et al. (2004)	Iliac	Tensile	Fibrous cap	Reported: stress-strain curves
			Fibrous intima	
			Fibrotic media	Ultimate stress and stretch
Loree et al. (1994)	Synthetic	Rheometer	Lipid pools	Reported: storage and loss moduli
Lee et al. (1991)	Aorta	Cyclic compressive	Fibrous cap	Reported: elastic moduli

the different constituents can largely be avoided. Studies utilizing nano-indentation (for example, Barrett et al. 2009) have shown large variation in local constituent mechanical properties, similar to that seen at the macroscopic level for the tissue as a whole. While useful for determining material properties in the physiological loading regime, indentation is limited when response to higher (supra-physiological) loads is being explored, including tissue rupture behavior.

It should be emphasized that it is necessary to determine plaque tissue mechanical behavior in both the physiological loading and supra-physiological loading regimes; the former is obviously relevant, but the latter is also of significant importance due, for example, to the high local strains and stresses caused by vascular device deployment and implantation.

Overall, looking into the future, mechanical testing and characterization of plaque tissue at the sub-structural scale is vitally important, to address the unmet need for more accurate atherosclerotic plaque constitutive and damage models.

For more information on these topics, the reader is referred to recent comprehensive review articles on plaque testing and mechanical properties (Cardoso and Weinbaum 2014) and the special issue on ‘Plaque Mechanics’ in the Journal of

biomechanics (Gijssen and Migliavacca 2014) that includes, for example, Akyildiz et al. (2014), Chai et al. (2014), Holzapfel et al. (2014), Kolandaivelu et al. (2014), Walsh et al. (2014).

4.3 Computational Modeling of Atherosclerotic Plaque

Based on the experimental mechanical property data that is available, constitutive models for plaque have been developed and implemented in computational models of atherosclerotic arteries. Linear elastic plaque representations have been developed (typically found in earlier studies) based on measured elastic modulus data. As an advancement on this, plaque tissue stress-strain curves have been used to calibrate a range of hyperelastic models in the finite deformation kinematics regime, and this is the most common approach reported in the literature to date. The majority of studies have assumed material isotropy for individual plaque constituents or the plaque as a whole where homogeneity and effective properties have been assumed. Anisotropy in fibrous tissue has also been explored. Table 2 gives a summary listing of reported computational studies involving atherosclerotic artery representations, where the studies have been categorized by spatial dimension (2D-planar or 3D), arterial geometry (idealized or realistic/patient specific, as might be determined from medical imaging), representation of the diseased tissue structure (whether homogenized or multi-component/multi-phase), and material model(s) employed. An illustrative example is that of Cilla et al. (2012) shown in Figs. 11 and 12, where a lipid core is represented using a hyperelastic idealization. In addition to this, the reader is referred to the aforementioned reviews for further information (in particular Holzapfel et al. 2014), and also Morlacchi and Migliavacca (2013).

4.3.1 Plaque Tissue Inelasticity and Damage Modeling

A significant limitation in current atherosclerotic plaque computational modeling is the accurate modeling of plaque inelasticity and damage. Clearly, significant challenges exist in characterizing plaque inelasticity and damage experimentally, going beyond difficulties associated with elastic and hyperelastic property identification. The small number of experimental studies that have investigated plaque inelasticity have shown the existence of inelastic/non-recoverable deformation (Topoleski et al. 1997; Topoleski and Salunke 2000; Ebenstein et al. 2009; Maher et al. 2011) depending on plaque type. Intimately linked with tissue inelasticity is tissue damage, not least because damage can manifest itself as inelastic deformation, with damage leading to material softening and rupture, and it is very clear from clinical practice that plaque can experience damage and rupture as part of the angioplasty procedure for example. As a consequence, there is a clear need for the accurate characterization of these phenomena (inelasticity, damage, softening and rupture) for the development of more accurate atherosclerotic artery computational models, in particular for the

Table 2 Computational modeling studies involving representation of atherosclerotic plaque

Reference	Type	Geometry	Constituents	Material model
Lee et al. (1992)	2D	Idealized	Plaque	Linear elastic
			Lipid pool	
Cheng et al. (1993)	2D	Realistic–Digitized tracing	Plaque	Linear elastic
			Lipid pool	
			Calcification	
Petrini et al. (2003)	3D	Idealized	Plaque	Hyperelastic 3rd order polynomial
Chua et al. (2004)	3D	Idealized	Plaque	Linear elastic
Migliavacca et al. (2004)	3D	Idealized	Plaque * 3 types	Hyperelastic 3rd order polynomial
Holzapfel et al. (2005b)	3D	Realistic—MRI scan	Diseased intima	Anisotropic hyperelastic
			Lipid pool	
			Calcification	
Li et al. (2006)	2D	Realistic—MRI scan	Fibrous cap	Hyperelastic ogden $n = 2$
			Lipid pool	
Migliavacca et al. (2007)	3D	Idealized	Plaque	Hyperelastic 3rd order polynomial
Kiousis et al. (2007)	3D	Realistic–MRI scan	Lipid pool	Hyperelastic
Timmins et al. (2008)	3D	Idealized	Plaque(stiffness varied)	Hyperelastic 3rd order polynomial
Bluestein et al. (2008)	3D	Idealized	Plaque	Hyperelastic Mooney–Rivlin
			Lipid pool	
			Calcification	
Tang et al. (2009a)	2D	Realistic–MRI scan	Plaque	Hyperelastic modified
			Lipid pool	Mooney–Rivlin
			Calcification	
Tang et al. (2009b)	3D	Realistic–MRI scan	Plaque	Hyperelastic modified
			Lipid pool	Mooney–Rivlin
			Calcification	
Pericevic et al. (2009)	3D	Idealized	Plaque * 3 types	Hyperelastic polynomial $n = 2$
Gastaldi et al. (2010)	3D	Idealized	Plaque	Hyperelastic polynomial $n = 2$

(continued)

Table 2 (continued)

Reference	Type	Geometry	Constituents	Material model
Gu et al. (2010)	3D	Idealized	Plaque	Hyperelastic polynomial $n = 2$
Sadat et al. (2010)	2D	Realistic–MRI scan	Plaque	Hyperelastic ogden $n = 2$
			Lipid pool	
			Calcification	
Zahedmanesh et al. (2010)	3D	Idealized	Plaque	Hyperelastic ogden $n = 1$
Wenk et al. (2010)	3D	Idealized	Fibrous tissue	Hyperelastic fung
			Lipid pool	
Pant et al. (2011)	3D	Idealized	Plaque	Hyperelastic neo-Hookean
Grogan et al. (2011)	3D	Idealized	Plaque	Hyperelastic polynomial $n = 6$
Wong et al. (2012)	2D	Realistic–MRI scan	Lipid pool	Linear elastic
			Fibrous cap	
			Calcification	
Cilla et al. (2012)	3D	Idealized	Lipid pool	Hyperelastic neo-Hookean
			Plaque	
García et al. (2012)	3D	Idealized	Lipid pool	Hyperelastic neo-Hookean
			Plaque	
			Calcification	
Conway et al. (2012)	3D	Idealized/Population specific	Plaque	Hyperelastic polynomial $n = 2$ Plastic (range of yield strengths)
Morlacchi et al. (2013)	3D	Realistic–CTA	Plaque	Hyperelastic polynomial $n = 6$
		Patient specific		Plastic (yield = 400 kPa)
Grogan et al. (2013)	3D	Idealized	Plaque	Hyperelastic polynomial $n = 2$
Morlacchi et al. (2014)	3D	Idealized	Plaque	Hyperelastic polynomial $n = 6$
			Calcification	

(continued)

Table 2 (continued)

Reference	Type	Geometry	Constituents	Material model
Iannaccone et al. (2014)	3D	Realistic	Fibrotic media	Anisotropic hyperelastic with continuum Damage model
			Lipid pool	
			Fibrous cap	
			Calcification	
Conway et al. (2014)	3D	Idealized/Population specific	Plaque	Hyperelastic polynomial $n = 2$, ogden $n = 1$ and $n = 6$, plasticity and pseudo-elasticity
			Lipid pool	
			Calcification	

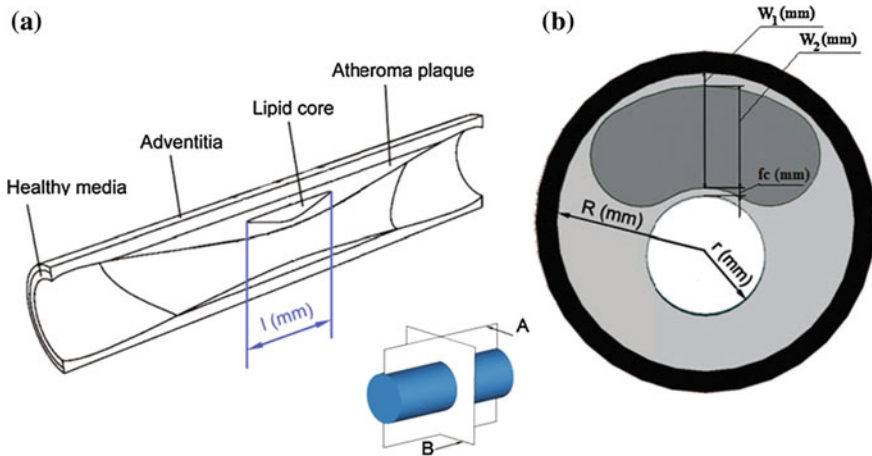


Fig. 11 Idealized geometry of an atherosclerotic arterial model (transversal section). Reproduced from Cilla et al. (2012) with permission

simulation of vascular interventions, such as balloon angioplasty, stent implantation and endarterectomy.

Inelasticity and Damage Modeling Approaches

Approaches reported in the literature for inelasticity and damage modeling include the following (Holzapfel et al. 2014).

The *fracture mechanics approach*, where plaque damage and rupture has been addressed as a crack initiation and growth problem, and some studies have used cohesive zone/interface debonding models to simulate material separation. Examples

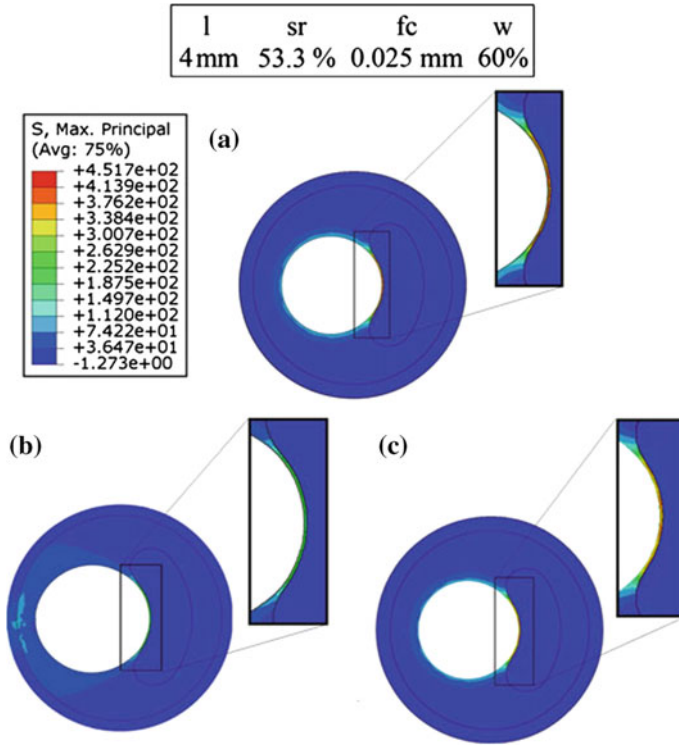


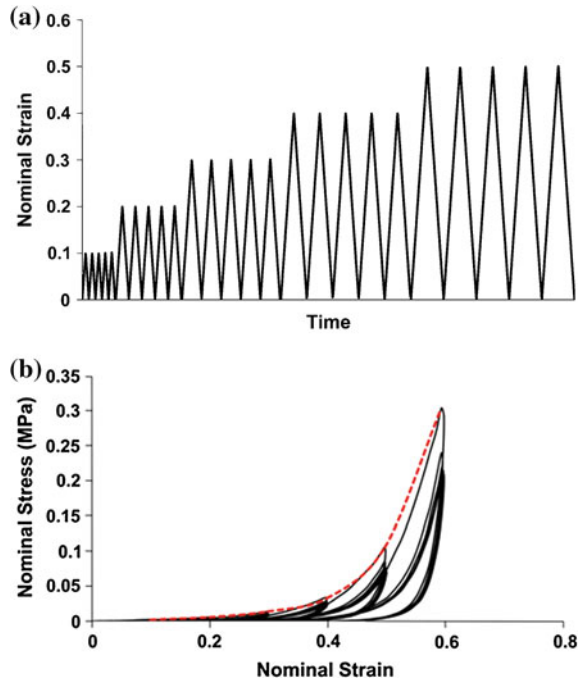
Fig. 12 Contour plots of the maximum principal stress with residual stresses included in (a) the longitudinal direction, (b) the longitudinal and circumferential directions, and (c) without either. Reproduced from Cilla et al. (2012) with permission

of studies in this category include: Versluis et al. (2006), Gasser and Holzapfel (2007), Ferrara and Pandolfi (2008), Nguyen and Levy (2010), Pei et al. (2013), McGarry et al. (2014), Máirtín et al. (2014). Most recently, Leng et al. (2015a, b) investigated the use of cohesive zone modeling to model the delamination of the plaque from the arterial wall.

The *continuum damage mechanics* approach, as described above in Sect. 3.3.1, where the plaque is simulated as a homogeneous continuum and with parameters introduced to represent permanent deformation (inelastic strain) and damage (damage parameter). Examples of studies in this category include Maher et al. (2011), Balzani et al. (2012), and Iannaccone et al. (2014).

The *pseudo-elasticity* and *elasto-plasticity* approaches have been used. The principle of the pseudo-elastic modeling approach has been described in Sect. 3.3.2, and has been used by Conway et al. (2014) to account for plaque damage in a computational

Fig. 13 Data on cyclic compression testing of atherosclerotic plaque samples (human carotid plaque) from Maher et al. (2011): incremental cyclic loading history (*upper figure*), and a typical stress–strain response (*lower figure the dotted line* represents the load envelope of the tissue). Reproduced with permission



model of stent angioplasty (see Sect. 5 below), motivated by the presence of the Mullins effect in experimental cyclic stress–strain data for plaque tissue (Maher et al. 2011) (see Fig. 13). In the elasto-plastic approach, to account primarily for tissue damage, the tissue has been idealized as an isotropic elastic-perfectly plastic material, where the plasticity is characterized by von Mises plasticity, with a yield stress determined from reported plaque stress–strain data. Examples of studies of this type are: Gastaldi et al. (2010), Conway et al. (2012, 2014), Morlacchi et al. (2013), where the Loree et al. (1994) data were used to identify a plaque yield stress of 400 kPa.

The continuum damage mechanics, pseudo-elasticity and elasto-plasticity modeling approaches are very useful phenomenological modeling approaches for attempting to incorporate plaque tissue damage into computational models. They are relatively easy to implement, as they are based on standard engineering mechanics modeling methods, and they do directly deal with the mechanical effects of damage in the tissue, viz., stress/load carrying capacity reduction (stress reduction/softening in the case of continuum damage mechanics and pseudo-elasticity, and stress limitation to the yield stress value in the case of elasto-plasticity). While attractive in terms of implementation, they are highly idealized and not physically based in terms of accounting directly for the microstructural deformation and failure mechanisms that are at play in the material, in particular given the structural heterogeneity of the material.

Plaque Rupture Stresses

In an attempt to characterize the mechanical strength of atherosclerotic plaque tissue, and to aid in assessing tissue rupture risk, significant attention has been paid in the literature to the identification of a 'plaque rupture stress'. These efforts have typically involved diseased arterial tissue mechanical testing, backed up by computational modeling, where the modeling is used to calculate the local peak tissue stress at the point of macroscopic tissue rupture, thereby identifying the rupture stress value (see Cardoso and Weinbaum 2014; Gijssen and Migliavacca 2014). Using such an approach, a very widely quoted plaque rupture stress threshold of 300 kPa was established by Cheng et al. (1993); they also reported an average rupture stress of 545 ± 160 kPa. The measure of stress used here was the peak circumferential stress (PCS), the local stress component in the arterial circumferential direction.

In terms of using such data in computational models to assess tissue rupture risk, arguably the best stress component to use generally to compare with these values is the maximum principal stress, since it could be argued that it is more representative of a critically loaded condition in a soft predominantly elastic fibrous material, in comparison to von Mises stress, for example, which is more representative of a critically loaded condition in predominantly plastically deforming materials that fail through shape distortion deformation modes (such as ductile metals). Nonetheless, useful critical von Mises stress data has also been reported for vulnerable plaque as lying between 227 and 683 kPa (Li et al. 2006).

Not surprisingly, rupture stresses have been found to be highly variable, depending on the plaque type examined; for example 342 kPa for lipid dominant plaque and 618 kPa for calcified plaque (Mulvihill et al. 2013). Weinbaum and co-workers (Maldonado et al. 2012; Kelly-Arnold et al. 2013; Cardoso and Weinbaum 2014) have focussed on the very important topic of vulnerable cap rupture stress, finding that the high stress concentrations around micro-calcifications (increasing stresses up to $\times 15$) could significantly lower effective rupture stresses for such tissue (see Fig. 14), below the nominal value of 300 kPa, with a value of 107 kPa reported in Maldonado et al. (2012).

4.4 Discussion and Limitations

Undoubtedly, despite the practical difficulties in relation to tissue sourcing and testing, significant and important experimental and modeling work has been performed to characterize and represent the mechanical behavior of atherosclerotic plaque. Significant insights into the mechanical performance of the tissue have been established, and models have been developed that have proven practically useful in computational modeling investigations of vascular interventions such as stent angioplasty.

However, significant work remains to be done on a number of fronts. Although difficult it would be very beneficial if a universally accepted standard for plaque material type could be established. It is clear, however, that this will only be possible

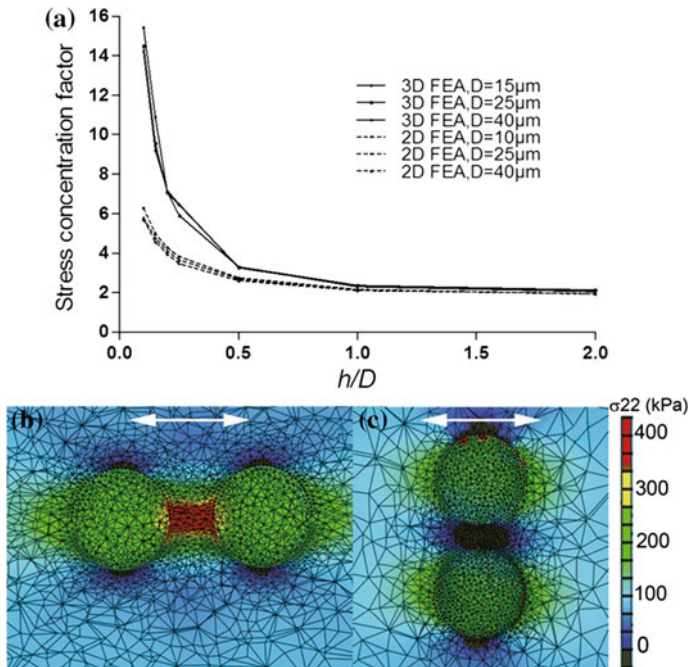


Fig. 14 **a** Illustrates the computational results for the analysis of stress concentrations caused by calcifications in a soft tissue matrix, and the relationship between the separation distance and the diameter, given by h and D , respectively. **b** and **c** show the finite element results for particles of h/D of 0.4 oriented along tensile and transverse loading axes, respectively (Kelly-Arnold et al. 2013). Reproduced with permission

when greater experimental characterization has been performed, but it would be hugely beneficial for the comparison of test data across different studies, and also for the development of constitutive models.

As indicated above, the modeling of plaque inelasticity and damage to date has primarily been phenomenological in nature, and while this is very useful for practical implementation in computational analysis and design studies, it is quite idealized and limited in its ability to accurately capture the details of material deformation and failure. Overall, improved and more physically based constitutive and damage model formulations are required (Holzapfel et al. 2014) that will be more physically accurate and representative in their mechanical performance predictions.

As part of this, multi-scale modeling (Gijssen and Migliavacca 2014) linking physically-based micromechanical modeling with macroscopic mechanical performance, to generate and calibrate more representative material constitutive and damage models, would be hugely beneficial. Current modeling efforts, where plaque tissue sub-structure has been modeled (e.g., Table 2), provide a roadmap for this, but focus needs to be given to more physically representative modeling of individual constituent behavior. In particular, focus needs to be applied to explicit representation of calcified particles and particle-matrix debonding as part of the damage process, the fluidic nature of the lipid pool, and matrix tissue anisotropy. The focus

of a number of recent studies on characterizing plaque calcification, and the effects of calcified particles on tissue mechanical response and rupture stresses, is particularly welcome in this regard (Maldonado et al. 2012; Kelly-Arnold et al. 2013; Cardoso and Weinbaum 2014; Barrett et al. 2016).

Further experimentation is required to more comprehensively characterize plaque tissue non-recoverable/plastic deformation, building on the limited work to date (Topoleski et al. 1997; Topoleski and Salunke 2000; Ebenstein et al. 2009; Maher et al. 2011), as this is essential for constitutive model development for use in computational modeling investigations of vascular interventions such as stent angioplasty, where tissue load-unload-reload behavior must be accurately captured.

Additionally, one area that has received little attention in the literature, in relation to experimental characterization and modeling, is plaque tissue loading rate dependence and viscoelasticity, although the existence of soft tissue viscoelasticity is well accepted. Indeed the tissue preconditioning cyclic loading that is widely utilized in mechanical testing programmes for soft tissue is largely intended to overcome tissue rate effects and viscoelasticity, and to produce stabilized stress–strain response curves for the testing programme proper. In relation to plaque tissue, Topoleski and Salunke (2000) report a significant time-dependent (stress-relaxation) response for the three plaque types that they considered (calcified, fibrous and atheromatous), indicating viscoelastic behavior, and they discuss the possibility that a plaque ‘opened during angioplasty may respond purely mechanically, reclosing after several days because of viscoelastic recovery in the tissue’. On this basis, further experimental work to obtain an accurate characterization of the rate dependence and viscoelasticity of plaque tissue would be extremely beneficial, with a view to accounting for such effects in constitutive and damage models. This would significantly enhance the capabilities of computational models, for example in relation to assessing the effects of balloon/stent deployment rate, and tissue strain recovery and stress relaxation over time.

In relation to future testing programmes, standardization of material storage, sample preparation and testing protocols would be very welcome, along the lines proposed by Walsh et al. (2014).

5 Applications in Stent Angioplasty

As is clear from the above sections, the development of tissue constitutive and damage models to enable the accurate computational modeling of vascular interventions, such as angioplasty, is of significant interest to the computational biomechanics community. This has, in part, been fueled by the industrial need for numerical simulation of medical device performance as part of medical device regulatory approval process, for example the US Food and Drug Administration (FDA 2010) requirements for the computational modeling of stent performance in angioplasty as part of their regulatory approval process.

While the literature on the computational modeling of stenting is vast, studies that have included explicit representations of plaque tissue sub-structure and constituents

are quite rare. This is surprising, given what is now known on the importance of having an accurate plaque tissue representation in computational models of this type, as reviewed in detail above. Examples of such studies include: Holzapfel et al. (2005b), García et al. (2012), Conway et al. (2014), Iannaccone et al. (2014), Morlacchi et al. (2014).

5.1 Stent Design Assessment—Population Specific Computational Modeling

As a practical application of the considerations discussed above, Conway et al. (2012, 2014) reported on the development of a computational test-bed for coronary angioplasty (using finite element analysis and the Abaqus software, Abaqus 2013) to facilitate stent mechanical performance assessment as part of the stent design process. In terms of overall arterial model geometry, the work proposed to bridge the gap between the use of highly idealized (straight or moderately curved cylindrical geometries) on the one hand, that have been extensively studied in the literature, and patient specific arterial geometries (generated from medical imaging) that have the limitation that they are by definition relevant for a particular individual, making generalizations difficult. Instead the population specific approach was taken where models for a range of geometrical population categories were created (covering variations in arterial curvature and stenosis level); this had the advantage of being more general than patient specific, yet more realistic than a single idealized arterial structure. The population specific arterial geometries are shown in Fig. 15, with the steps in the stent deployment simulation illustrated in Fig. 16.

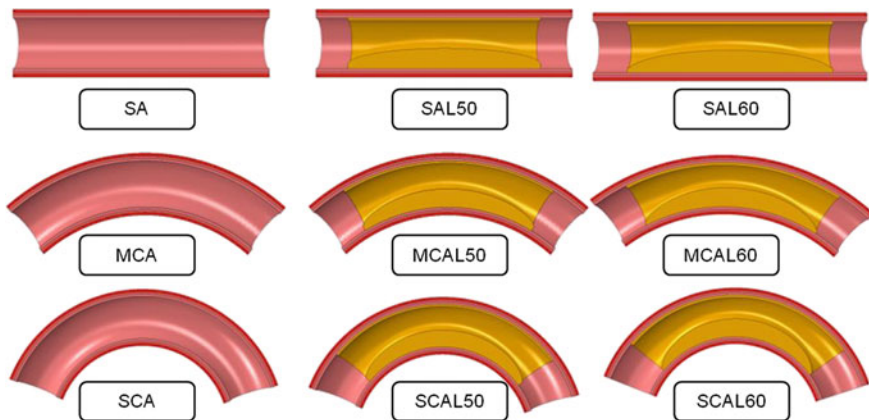
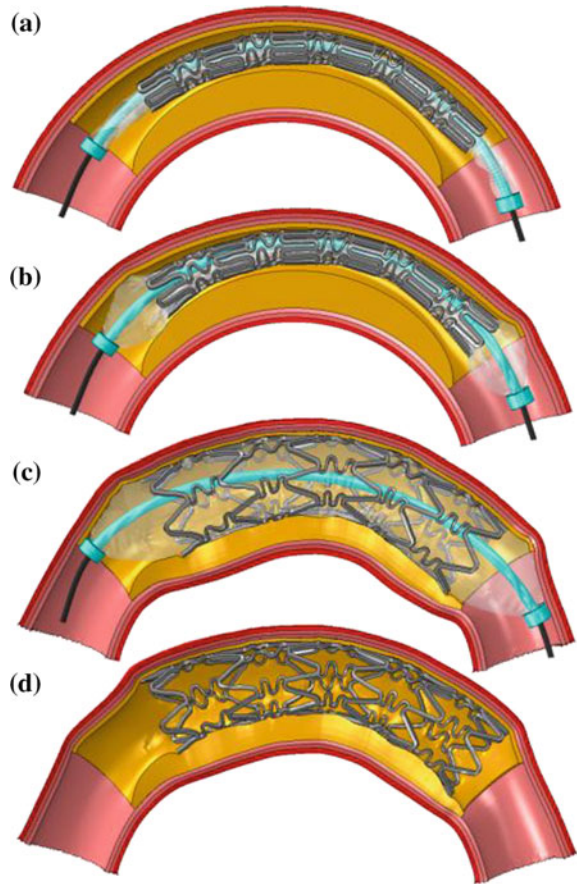


Fig. 15 The population-specific arterial geometries of Conway et al. (2012), covering three levels of curvature (straight artery SA, moderately curved artery MCA, severely curved artery SCA) and three stenosis levels (no stenosis, 50% lesion L50, 60% lesion L60). The curvature is quantified by the tortuosity index (TI), with values 0.0, 0.1, 0.3, reading from the *top* to the *bottom* row (Serruys 2008). Reproduced with permission

Fig. 16 Simulation of the steps in stent deployment simulation from Conway et al. (2012). **a** Pre-deployment; **b** mid-deployment; **c** maximum balloon inflation; **d** post balloon deflation and removal. Case considered is a severely curved artery with 60% lesion (SCAL60), and the Cypher-like stent. Reproduced with permission



A second motivation of the work was to attempt to better inform regulatory body guidelines for medical device approval, in particular the FDA guidelines on computational modeling of stent performance in angioplasty (US Food and Drug Administration, FDA 2010). It is interesting to note that these guidelines are relatively imprecise in terms of prescribing details on the diseased artery model structure and the range of arterial geometries that should be considered in these analyzes to generate an accurate depiction of device performance in vivo.

Within the geometrical framework shown in Fig. 15 a three-layer arterial model (intima, media, adventitia) was implemented using the HGO model described above, with material constants as established in Holzapfel et al. (2005a, b). A wide range of stenotic (plaque) tissue representations were considered. In Conway et al. (2012) the tissue was represented as a homogeneous nonlinear elastic–plastic material with the nonlinear elasticity characterized by a Mooney–Rivlin polynomial hyperelastic model calibrated by Pericevic et al. (2009) to the Loree et al. (1994) experimental data; a range of plaque tissue types (cellular, hypocellular, calcified) with a range of

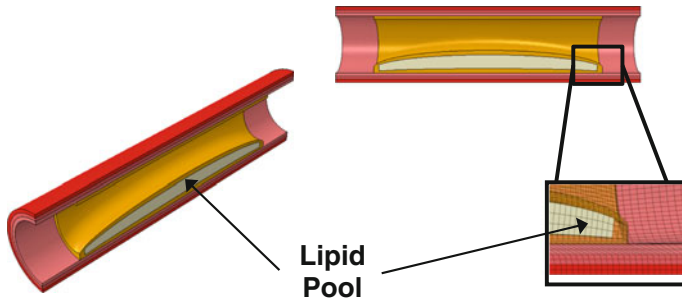


Fig. 17 Schematic diagram of SAL50 artery model (Fig. 15) with lipid pool, constituting 9.3% of total atherosclerotic tissue volume (Conway et al. 2014). Reproduced with permission

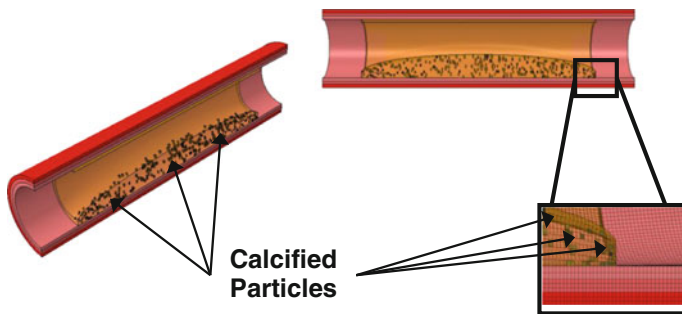


Fig. 18 Schematic diagram of SAL50 artery model (Fig. 15) with calcified particles, constituting 0.5% of total atherosclerotic tissue volume (Conway et al. 2014). Reproduced with permission

plastic yield stresses (to represent plaque tissue damage) derived from the Loree et al. (1994) data were used. As test cases, the computational test-bed was applied to two stent geometries, based on the closed-cell Cypher stent and the open-cell Multi-Link stent. In Conway et al. (2014) particular focus was applied to the plaque representation to include multiple constituents and constituent combinations, including matrix tissue, lipid pool (Fig. 17) and calcified particles (Fig. 18). In addition, a range of matrix tissue representations was considered, ranging from very soft tissue (using a first-order Ogden hyperelastic model, calibrated from Maher et al. (2011) compressive stress–strain data) to significantly stiffer tissue (using the Mooney–Rivlin polynomial model calibration from Conway et al. 2012). Finally, two plaque (matrix) tissue damage representations were considered: elasto-plasticity (as per Conway et al. 2012) and pseudo-elasticity (using the Ogden and Roxburgh 1999 model, calibrated to the Maher et al. 2011 data—see Fig. 13). This computational test-bed formulation allowed for the effects of each of the modeling features and variations to be considered, and insight gained into their relative importance for the practical purpose of stent mechanical performance assessment, which in turn was assessed through the following measures: stented vessel recoil, stent scaffolding capability (related to radial strength) and tissue damage risk (related to peak tissue stress levels generated).

As detailed in Conway et al. (2012, 2014) the results generated were highly insightful. In relation to overall arterial geometry (Fig. 15), one surprising result was that arterial curvature had only a minor influence on the stent performance measures; relatively speaking, the stenosis level dominated the model predictions, controlling the differentiation between the performance of the two stents (with the open-cell design performing better for larger stenosis levels, and also for greater arterial tortuosity), leading to the suggestion that stenosis level could be critically important parameter in stent selection for the clinician.

Leading on from this, in addition to stenosis level (plaque size), the constitutive description of the plaque tissue, and its sub-structure details, were seen to be extremely influential in determining stent performance, and it was possible to infer relative importance across the range of plaque tissue modeling features considered. In this context, the choice of plaque tissue matrix properties was seen to dominate the results, indicating the importance of establishing clearly defined plaque tissue types, and achieving accurate experimental mechanical characterization that is tissue-type dependent. In relation to damage modeling, the elasto-plasticity approach was significantly more influential than the pseudo-elasticity approach, and this could be related to the significant peak stress limiting effect of the plasticity model on the loading and reloading path, relative to the pseudo-elastic model. This clearly indicates the need to accurately capture the stress softening effects of tissue damage in constitutive models. In relation to plaque tissue sub-structure representation, the presence of calcifications dominated over the presence of the lipid pool in determining stent performance, through increasing vessel recoil (reducing lumen gain) and increasing local tissue stresses (Fig. 19, and in particular Fig. 19f), with the lipid pool only being influential in very soft matrix tissue cases; this emphasizes the importance of having an accurate representation of calcified particles in the plaque tissue model, which is consistent with the recent enhanced focus on characterizing the mechanical effects of plaque tissue calcification, as noted above in Sect. 4.4 (Maldonado et al. 2012; Kelly-Arnold et al. 2013; Cardoso and Weinbaum 2014; Barrett et al. 2016).

One interesting observation was the degree to which plaque tissue is subjected to multi-axial stresses, including both tension and compression, indicating the need for experimental characterization of plaque tissue under multi-axial loading conditions to drive the development of sufficiently representative constitutive and damage models.

5.2 Recommendations on Regulatory Body Guidelines

The results of the Conway et al. (2012, 2014) studies are of value from the perspective of informing regulatory body guidelines on numerical simulation of stent performance as part of the medical device regulatory approval process. In the current FDA guidelines document (US Food and Drug Administration, FDA 2010) there is no specific requirement to include an atherosclerotic stenosis or to vary its geometry or constitutive representation in such numerical simulations. However, based on the

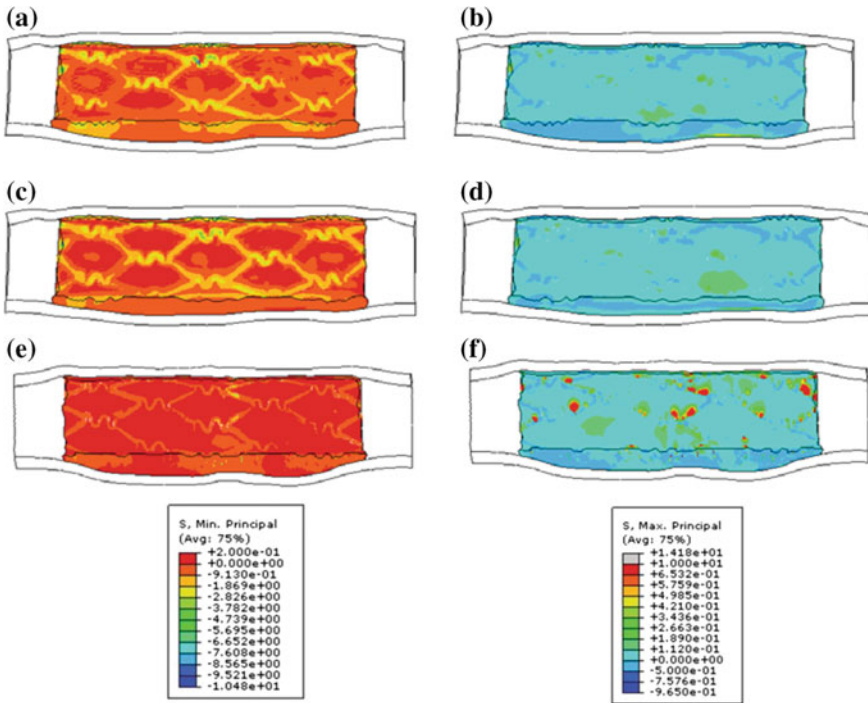


Fig. 19 Principal stress contour plots (MPa) in the plaque tissue at maximum balloon inflation, for the soft Ogden matrix tissue model and the Cypher-like stent (Conway et al. 2014). Minimum principal stresses (a, c, e); maximum principal stresses (b, d, f); lipid pool (c, d); calcifications (e, f). Reproduced with permission

present computational test-bed simulation results, it is strongly recommended that the guidelines on computational modeling of stent performance should be updated to:

- Require the inclusion of plaque tissue in such models and the assessment of stent performance over a range of plaque tissue volumes, consistent with the target diseased artery state.
- Require plaque tissue matrix elasticity to be varied over a range (stiff to compliant) that is consistent with the target diseased artery state, and that plaque tissue constituents such as calcifications (in particular) and lipid pools be included.
- Require plaque tissue damage to be represented in such models, perhaps using a plasticity representation (due in part to ease of implementation), until more physically representative models become established.
- Retain the representation of vessel curvature, adhering to the current guideline curvature levels as a minimum. While its influence was seen to be less influential in the test-bed simulations, its presence is nonetheless important to include when different stent designs are being compared.

6 Overall Conclusions

As this chapter has hopefully set out, outstanding progress has been made over (circa) the last twenty years in the characterization of the biomechanics of healthy and diseased vascular tissue, and in the use of such knowledge and data to develop mathematical models (analytical and computational) that can be of significant benefit in the analysis of vascular intervention procedures and in the analysis and design of vascular implants and devices. This has undoubtedly been fueled by rapid advances in imaging and characterization methodologies, and in computational power and simulation software development.

Nevertheless challenges still exist, in particular in relation to the plaque tissue, to more accurately characterize tissue mechanical behavior and quantify tissue mechanical properties, and from this to develop enhanced physically based constitutive and damage models. In relation to the latter, multi-scale modeling methods show promise, given that features and phenomena at different length scales in the material, such as micro- (and nano-) calcifications, calcified particle-matrix debonding, matrix tissue anisotropy and tissue inter-layer debonding, etc., can be explicitly represented, and their effects interrelated, in computational models.

Such developments will continue to enhance the power of computational models to be of significant importance in the analysis, design, and performance assessment of next generation vascular implants, such as biodegradable stents (Grogan et al. 2011, 2013; Boland et al. 2015; McHugh et al. 2015) and stents for peripheral and neural applications.

Acknowledgments The authors acknowledge funding from the Irish Research Council (IRC) under the Embark Initiative (C. Conway), the NUI Galway College of Engineering and Informatics (B. O'Reilly), the SFI/HEA Irish Centre for High-End Computing (ICHEC) and the Programme for Research in Third-Level Institutions (PRTL) Cycle 5 and co-funded under the European Regional Development Fund (ERDF).

References

- Abaqus, Dassault Systèmes, Simulia, Providence, RI, USA (2013)
- Akyildiz, A.C., Speelman, L., Gijssen, F.J.: Mechanical properties of human atherosclerotic intima tissue. *J. Biomech.* **47**, 773–783 (2014)
- Alastrué, V., Rodríguez, J.F., Calvo, B., Doblaré, M.: Structural damage models for fibrous biological soft tissues. *Int. J. Solids Struct.* **44**, 5894–5911 (2007)
- Balzani, D., Schröder, J., Gross, D.: A simple model for anisotropic damage with applications to soft tissues. *PAMM* **4**, 236–237 (2004)
- Balzani, D., Schröder, J., Gross, D.: Simulation of discontinuous damage incorporating residual stresses in circumferentially overstretched atherosclerotic arteries. *Acta Biomater.* **2**, 609–618 (2006)
- Balzani, D., Brinkhues, S., Holzapfel, G.A.: Constitutive framework for the modeling of damage in collagenous soft tissues with application to arterial walls. *Comput. Methods Appl. Mech. Eng.* **213**, 139–151 (2012)

- Barrett, H.E., Cunnane, E.M., Kavanagh, E.G., Walsh, M.T.: On the effect of calcification volume and configuration on the mechanical behaviour of carotid plaque tissue. *J. Mech. Behav. Biomed. Mater.* **56**, 45–56 (2016)
- Barrett, S.R., Sutcliffe, M.P., Howarth, S., Li, Z.Y., Gillard, J.H.: Experimental measurement of the mechanical properties of carotid atherothrombotic plaque fibrous cap. *J. Biomech.* **42**, 1650–1655 (2009)
- Bluestein, D., Alemu, Y., Avrahami, I., Gharib, M., Dumont, K., Ricotta, J.J., Einav, S.: Influence of microcalcifications on vulnerable plaque mechanics using FSI modeling. *J. Biomech.* **41**, 1111–1118 (2008)
- Boland, E.L., Shine, R., Kelly, N., Sweeney, C.A., McHugh, P.E.: A review of material degradation modelling for the analysis and design of bioabsorbable stents. *Ann. Biomed. Eng.* **44**, 341–356 (2015)
- Brinkhues, S., Balzani, D., Holzapfel, G.A.: Simulation of damage hysteresis in soft biological tissues. *PAMM* **9**, 155–156 (2009)
- Calvo, B., Peña, E., Martínez, M.A., Doblaré, M.: An uncoupled directional damage model for fibred biological soft tissues. Formulation and computational aspects. *Int. J. Numer. Methods Eng.* **69**, 2036–2057 (2007)
- Cardoso, L., Weinbaum, S.: Changing views of the biomechanics of vulnerable plaque rupture: a review. *Ann. Biomed. Eng.* **42**, 415–431 (2014)
- Chai, C.-K., Akyildiz, A.C., Speelman, L., Gijssen, F.J., Oomens, C.W., van Sambeek, M.R., van der Lugt, A., Baaijens, F.P.: Local axial compressive mechanical properties of human carotid atherosclerotic plaques-characterisation by indentation test and inverse finite element analysis. *J. Biomech.* **46**, 1759–1766 (2013)
- Chai, C.-K., Speelman, L., Oomens, C.W., Baaijens, F.P.: Compressive mechanical properties of atherosclerotic plaques-Indentation test to characterise the local anisotropic behaviour. *J. Biomech.* **47**, 784–792 (2014)
- Cheng, G.C., Loree, H.M., Kamm, R.D., Fishbein, M.C., Lee, R.T.: Distribution of circumferential stress in ruptured and stable atherosclerotic lesions. A structural analysis with histopathological correlation. *Circulation* **87**, 1179–1187 (1993)
- Chua, S.N.D., MacDonald, B.J., Hashmi, M.S.J.: Finite element simulation of slotted tube (stent) with the presence of plaque and artery by balloon expansion. *J. Mater. Process. Technol.* **155**, 1772–1779 (2004)
- Ciarletta, P., Dario, P., Micera, S.: Pseudo-hyperelastic model of tendon hysteresis from adaptive recruitment of collagen type I fibrils. *Biomaterials* **29**, 764–770 (2008)
- Cilla, M., Peña, E., Martínez, M.A.: 3D computational parametric analysis of eccentric atheroma plaque: influence of axial and circumferential residual stresses. *Biomech. Model. Mechanobiol.* **11**, 1001–1013 (2012)
- Conway, C.: The development of a computational test-bed to assess coronary stent implantation. Ph.D. thesis, National University of Ireland, Galway (2013)
- Conway, C., Sharif, F., McGarry, J.P., McHugh, P.E.: A computational test-bed to assess coronary stent implantation mechanics using a population-specific approach. *Cardiovasc. Eng. Technol.* **3**, 374–387 (2012)
- Conway, C., McGarry, J.P., McHugh, P.E.: Modelling of atherosclerotic plaque for use in a computational test-bed for stent angioplasty. *Ann. Biomed. Eng.* **42**, 2425–2439 (2014)
- Creane, A.: Identification of potential clinical indicators of carotid plaque disruption using patient specific finite element modelling. Ph.D. thesis, Dublin City University (2011)
- Creane, A., Maher, E., Sultan, S., Hynes, N., Kelly, D.J., Lally, C.: A remodelling metric for angular fibre distributions and its application to diseased carotid bifurcations. *Biomech. Model. Mechanobiol.* **11**, 869–882 (2012)
- Dorfmann, A., Ogden, R.W.: A pseudo-elastic model for loading, partial unloading and reloading of particle-reinforced rubber. *Int. J. Solids Struct.* **40**, 2699–2714 (2003)
- Dorfmann, A., Ogden, R.W.: A constitutive model for the Mullins effect with permanent set in particle-reinforced rubber. *Int. J. Solids Struct.* **41**, 1855–1878 (2004)

- Driessen, N.J., Wilson, W., Bouten, C.V., Baaijens, F.P.: A computational model for collagen fibre remodelling in the arterial wall. *J. Theor. Biol.* **226**, 53–64 (2004)
- Ebenstein, D.M., Coughlin, D., Chapman, J., Li, C., Pruitt, L.A.: Nanomechanical properties of calcification, fibrous tissue, and hematoma from atherosclerotic plaques. *J. Biomed. Mater. Res.* **A 91**, 1028–1037 (2009)
- Ehret, A.E., Itskov, M.: Modeling of anisotropic softening phenomena: application to soft biological tissues. *Int. J. Plast.* **25**, 901–919 (2009)
- FDA: Non-Clinical Engineering Tests and Recommended Labeling for Intravascular Stents and Associated Delivery Systems. Printable version (2010). <http://www.fda.gov/medicaldevices/deviceregulationandguidance/guidancedocuments/ucm071863.htm>
- Ferrara, A., Pandolfi, A.: Numerical modelling of fracture in human arteries. *Comput. Meth. Biomech. Biomed. Eng.* **11**, 553–567 (2008)
- Franceschini, G., Bigoni, D., Regitnig, P., Holzapfel, G.A.: Brain tissue deforms similarly to filled elastomers and follows consolidation theory. *J. Mech. Phys. Solids* **54**, 2592–2620 (2006)
- García, A., Peña, E., Martínez, M.A.: Influence of geometrical parameters on radial force during self-expanding stent deployment. Application for a variable radial stiffness stent. *J. Mech. Behav. Biomed. Mater.* **10**, 166–175 (2012)
- Gasser, T.C.: An irreversible constitutive model for fibrous soft biological tissue: a 3-D microfiber approach with demonstrative application to abdominal aortic aneurysms. *Acta Biomater.* **7**, 2457–2466 (2011)
- Gasser, T.C., Holzapfel, G.A.: Modeling plaque fissuring and dissection during balloon angioplasty intervention. *Ann. Biomed. Eng.* **35**, 711–723 (2007)
- Gasser, T.C., Ogden, R.W., Holzapfel, G.A.: Hyperelastic modelling of arterial layers with distributed collagen fibre orientations. *J. R. Soc. Interface* **3**, 15–35 (2006)
- Gastaldi, D., Morlacchi, S., Nichetti, R., Capelli, C., Dubini, G., Petrini, L., Migliavacca, F.: Modelling of the provisional side-branch stenting approach for the treatment of atherosclerotic coronary bifurcations: effects of stent positioning. *Biomech. Model. Mechanobiol.* **9**, 551–561 (2010)
- Gijzen, F.J., Migliavacca, F.: Plaque mechanics. *J. Biomech.* **4**, 763–764 (2014)
- Gracia, L.A., Peña, E., Royo, J.M., Pelegay, J.L., Calvo, B.: A comparison between pseudo-elastic and damage models for modelling the Mullins effect in industrial rubber components. *Mech. Res. Commun.* **36**, 769–776 (2009)
- Grogan, J.A., O'Brien, B.J., Leen, S.B., McHugh, P.E.: A corrosion model for bioabsorbable metallic stents. *Acta Biomater.* **7**, 3523–3533 (2011)
- Grogan, J.A., Leen, S.B., McHugh, P.E.: Optimizing the design of a bioabsorbable metal stent using computer simulation methods. *Biomaterials* **34**, 8049–8060 (2013)
- Gu, L., Zhao, S., Muttyam, A.K., Hammel, J.M.: The relation between the arterial stress and restenosis rate after coronary stenting. *J. Med. Devices* **4**, 031005 (2010)
- Hariton, I., de Botton, G., Gasser, T.C., Holzapfel, G.A.: Stress-driven collagen fiber remodeling in arterial walls. *Biomech. Model. Mechanobiol.* **6**, 163–175 (2007)
- Hokanson, J., Yazdani, S.: A constitutive model of the artery with damage. *Mech. Res. Commun.* **24**, 151–159 (1997)
- Holzapfel, G.A., Gasser, T.C., Ogden, R.W.: A new constitutive framework for arterial wall mechanics and a comparative study of material models. *J. Elast.* **61**, 1–48 (2000)
- Holzapfel, G.A., Sommer, G., Regitnig, P.: Anisotropic mechanical properties of tissue components in human atherosclerotic plaques. *J. Biomech. Eng.* **126**, 657–665 (2004)
- Holzapfel, G.A., Sommer, G., Gasser, C.T., Regitnig, P.: Determination of layer-specific mechanical properties of human coronary arteries with nonatherosclerotic intimal thickening and related constitutive modeling. *Am. J. Physiol.-Heart Circ. Physiol.* **289**, H2048–H2058 (2005a)
- Holzapfel, G.A., Stadler, M., Gasser, T.C.: Changes in the mechanical environment of stenotic arteries during interaction with stents: computational assessment of parametric stent designs. *J. Biomech. Eng.* **127**, 166–180 (2005b)
- Holzapfel, G.A., Mulvihill, J.J., Cunnane, E.M., Walsh, M.T.: Computational approaches for analyzing the mechanics of atherosclerotic plaques: a review. *J. Biomech.* **47**, 859–869 (2014)

- Iannaccone, F., Debusschere, N., De Bock, S., De Beule, M., Van Loo, D., Vermassen, F., Segers, P., Verheghe, B.: The influence of vascular anatomy on carotid artery stenting: a parametric study for damage assessment. *J. Biomech.* **47**, 890–898 (2014)
- Kelly-Arnold, A., Maldonado, N., Laudier, D., Aikawa, E., Cardoso, L., Weinbaum, S.: Revised microcalcification hypothesis for fibrous cap rupture in human coronary arteries. *Proc. Nat. Acad. Sci.* **110**, 10741–10746 (2013)
- Kiousis, D.E., Gasser, T.C., Holzappel, G.A.: A numerical model to study the interaction of vascular stents with human atherosclerotic lesions. *Ann. Biomed. Eng.* **35**, 1857–1869 (2007)
- Kolandaivelu, K., Leiden, B.B., Edelman, E.R.: Predicting response to endovascular therapies: dissecting the roles of local lesion complexity, systemic comorbidity, and clinical uncertainty. *J. Biomech.* **47**, 908–921 (2014)
- Lawlor, M.G., O'Donnell, M.R., O'Connell, B.M., Walsh, M.T.: Experimental determination of circumferential properties of fresh carotid artery plaques. *J. Biomech.* **44**, 1709–1715 (2011)
- Lee, R.T., Grodzinsky, A.J., Frank, E.H., Kamm, R.D., Schoen, F.J.: Structure-dependent dynamic mechanical behavior of fibrous caps from human atherosclerotic plaques. *Circulation* **83**, 1764–1770 (1991)
- Lee, R.T., Richardson, S.G., Loree, H.M., Grodzinsky, A.J., Gharib, S.A., Schoen, F.J., Pandian, N.: Prediction of mechanical properties of human atherosclerotic tissue by high-frequency intravascular ultrasound imaging. An in vitro study. *Arterioscler. Thromb.* **12**, 1–5 (1992)
- Leng, X., Chen, X., Deng, X., Sutton, M.A., Lessner, S.M.: Modeling of experimental atherosclerotic plaque delamination. *Ann. Biomed. Eng.* **43**, 2838–2851 (2015a)
- Leng, X., Chen, X., Deng, X., Sutton, M.A., Lessner, S.M.: Simulation of atherosclerotic plaque delamination using the cohesive zone model. In: Barthelat, F., Korach, C., Zavatierrri, P., Prorok, B.C., Grande-Allen, K.J. (eds.) *Mechanics of Biological Systems and Materials*, vol. 7, pp. 81–88. Springer, Berlin (2015b)
- Li, Z.-Y., Howarth, S., Trivedi, R.A.: U-King-Im, J.M., Graves, M.J., Brown, A., Wang, L., Gillard, J.H.: Stress analysis of carotid plaque rupture based on in vivo high resolution MRI. *J. Biomech.* **39**, 2611–2622 (2006)
- Loree, H.M., Grodzinsky, A.J., Park, S.Y., Gibson, L.J., Lee, R.T.: Static circumferential tangential modulus of human atherosclerotic tissue. *J. Biomech.* **27**, 195–204 (1994)
- Maher, E., Creane, A., Sultan, S., Hynes, N., Lally, C., Kelly, D.J.: Tensile and compressive properties of fresh human carotid atherosclerotic plaques. *J. Biomech.* **42**, 2760–2767 (2009)
- Maher, E., Creane, A., Sultan, S., Hynes, N., Lally, C., Kelly, D.J.: Inelasticity of human carotid atherosclerotic plaque. *Ann. Biomed. Eng.* **39**, 2445–2455 (2011)
- Maher, E., Creane, A., Lally, C., Kelly, D.J.: An anisotropic inelastic constitutive model to describe stress softening and permanent deformation in arterial tissue. *J. Mech. Behav. Biomed. Mater.* **12**, 9–19 (2012)
- Máirtín, É.Ó., Parry, G., Beltz, G.E., McGarry, J.P.: Potential-based and non-potential-based cohesive zone formulations under mixed-mode separation and over-closure-Part II: Finite element applications. *J. Mech. Phys. Solids* **63**, 363–385 (2014)
- Maldonado, N., Kelly-Arnold, A., Vengrenyuk, Y., Laudier, D., Fallon, J.T., Virmani, R., Cardoso, L., Weinbaum, S.: A mechanistic analysis of the role of microcalcifications in atherosclerotic plaque stability: potential implications for plaque rupture. *Am. J. Physiol.-Heart Circ. Physiol.* **303**, H619–H628 (2012)
- Martin, C., Sun, W.: Modeling of long-term fatigue damage of soft tissue with stress softening and permanent set effects. *Biomech. Model. Mechanobiol.* **12**, 645–655 (2013)
- McGarry, J.P., Máirtín, É.Ó., Parry, G., Beltz, G.E.: Potential-based and non-potential-based cohesive zone formulations under mixed-mode separation and over-closure. Part I: Theoretical analysis. *J. Mech. Phys. Solids* **63**, 336–362 (2014)
- McHugh, P.E., Grogan, J.A., Conway, C., Boland, E.: Computational modeling for analysis and design of metallic biodegradable stents. *J. Med. Devices* **9**, 030946 (2015)
- Miehe, C.: Discontinuous and continuous damage evolution in Ogden-type large-strain elastic materials. *Eur. J. Mech.-A/Solids* **14**, 697–720 (1995)

- Migliavacca, F., Petrini, L., Massarotti, P., Schievano, S., Auricchio, F., Dubini, G.: Stainless and shape memory alloy coronary stents: a computational study on the interaction with the vascular wall. *Biomech. Model. Mechanobiol.* **2**, 205–217 (2004)
- Migliavacca, F., Gervaso, F., Prosi, M., Zunino, P., Minisini, S., Formaggia, L., Dubini, G.: Expansion and drug elution model of a coronary stent. *Comput. Meth. Biomech. Biomed. Eng.* **10**, 63–73 (2007)
- Morlacchi, S., Migliavacca, F.: Modeling stented coronary arteries: where we are, where to go. *Ann. Biomed. Eng.* **41**, 1428–1444 (2013)
- Morlacchi, S., Colleoni, S.G., Cárdenes, R., Chiastrì, C., Diez, J.L., Larrabide, I., Migliavacca, F.: Patient-specific simulations of stenting procedures in coronary bifurcations: two clinical cases. *Med. Eng. Phys.* **35**, 1272–1281 (2013)
- Morlacchi, S., Pennati, G., Petrini, L., Dubini, G., Migliavacca, F.: Influence of plaque calcifications on coronary stent fracture: a numerical fatigue life analysis including cardiac wall movement. *J. Biomech.* **47**, 899–907 (2014)
- Mulvihill, J.J., Cunnane, E.M., McHugh, S.M., Kavanagh, E.G., Walsh, S.R., Walsh, M.T.: Mechanical, biological and structural characterization of in vitro ruptured human carotid plaque tissue. *Acta Biomater.* **9**, 9027–9035 (2013)
- Nolan, D.R., Gower, A.L., Destrade, M., Ogden, R.W., McGarry, J.P.: A robust anisotropic hyper-elastic formulation for the modelling of soft tissue. *J. Mech. Behav. Biomed. Mater.* **39**, 48–60 (2014)
- Nolan, D.R., McGarry, J.P.: On the compressibility of arterial tissue. *Ann. Biomed. Eng.* (2015) (in Press). doi:[10.1007/s10439-015-1417-1](https://doi.org/10.1007/s10439-015-1417-1)
- Nguyen, C.M., Levy, A.J.: The mechanics of atherosclerotic plaque rupture by inclusion/matrix interfacial decohesion. *J. Biomech.* **43**, 2702–2708 (2010)
- Ogden, R.W., Roxburgh, D.G.: A pseudo-elastic model for the Mullins effect in filled rubber. *Proc. R. Soc. Lond. A* **455**, 2861–2877 (1999)
- Pant, S., Limbert, G., Curzen, N.P., Bressloff, N.W.: Multiobjective design optimisation of coronary stents. *Biomaterials* **32**, 7755–7773 (2011)
- Pei, X., Wu, B., Li, Z.-Y.: Fatigue crack propagation analysis of plaque rupture. *J. Biomech. Eng.* **135**, 101003 (2013)
- Peña, E.: A rate dependent directional damage model for fibred materials: application to soft biological tissues. *Comput. Mech.* **48**, 407–420 (2011)
- Peña, E., Doblaré, M.: An anisotropic pseudo-elastic approach for modelling Mullins effect in fibrous biological materials. *Mech. Res. Commun.* **36**, 784–790 (2009)
- Peña, E., Martins, P., Mascarenhas, T., Natal Jorge, R.M., Ferreira, A., Doblaré, M., Calvo, B.: Mechanical characterization of the softening behavior of human vaginal tissue. *J. Mech. Behav. Biomed. Mater.* **4**, 275–283 (2011)
- Pericevic, I., Lally, C., Toner, D., Kelly, D.J.: The influence of plaque composition on underlying arterial wall stress during stent expansion: the case for lesion-specific stents. *Med. Eng. Phys.* **31**, 428–433 (2009)
- Peña, E., Peña, J.A., Doblaré, M.: On the Mullins effect and hysteresis of fibered biological materials: a comparison between continuous and discontinuous damage models. *Int. J. Solids Struct.* **46**, 1727–1735 (2009)
- Petrini, L., Migliavacca, F., Dubini, G., Auricchio, F.: Numerical analysis of vascular stents exploiting shape-memory-alloy behavior. In: 16th AIMETA Congress of the Theoretical and Applied Mechanics, pp. 1–10 (2003)
- Rodríguez, J.F., Cacho, F., Bea, J.A., Doblaré, M.: A stochastic-structurally based three dimensional finite-strain damage model for fibrous soft tissue. *J. Mech. Phys. Solids* **54**, 864–886 (2006)
- Rodríguez, J.F., Alastrué, V., Doblaré, M.: Finite element implementation of a stochastic three dimensional finite-strain damage model for fibrous soft tissue. *Comput. Meth. Appl. Mech. Eng.* **197**, 946–958 (2008)
- Sadat, U., Li, Z.-Y., Young, V.E., Graves, M.J., Boyle, J.R., Warburton, E.A., Varty, K., O'Brien, E., Gillard, J.H.: Finite element analysis of vulnerable atherosclerotic plaques: a comparison

- of mechanical stresses within carotid plaques of acute and recently symptomatic patients with carotid artery disease. *J. Neurol. Neurosurg. Psychiatry* **81**, 286–289 (2010)
- Salunke, N.V., Topoleski, L.D., Humphrey, J.D., Mergner, W.J.: Compressive stress-relaxation of human atherosclerotic plaque. *J. Biomed. Mater. Res.* **55**, 236–241 (2001)
- Serruys, P.W., Onuma, Y., Morel, M.: CAAS 2D/3D QCA Bifurcation analysis approach. European Bifurcation Club, Prague (2008)
- Stary, H.C.: *Atlas of Atherosclerosis: Progression and Regression*, 1st edn. CRC Press, New York (1999)
- Tang, D., Teng, Z., Canton, G., Hatsukami, T.S., Dong, L., Huang, X., Yuan, C.: Local critical stress correlates better than global maximum stress with plaque morphological features linked to atherosclerotic plaque vulnerability: an in vivo multi-patient study. *Biomed. Eng. Online* **8**, 15 (2009a). doi:[10.1186/1475-925X-8-15](https://doi.org/10.1186/1475-925X-8-15)
- Tang, D., Yang, C., Kobayashi, S., Zheng, J., Woodard, P.K., Teng, Z., Billiar, K., Bach, R., Ku, D.N.: 3D MRI-based anisotropic FSI models with cyclic bending for human coronary atherosclerotic plaque mechanical analysis. *J. Biomech. Eng.* **131**, 061010 (2009b)
- Teng, Z., Tang, D., Zheng, J., Woodard, P.K., Hoffman, A.H.: An experimental study on the ultimate strength of the adventitia and media of human atherosclerotic carotid arteries in circumferential and axial directions. *J. Biomech.* **42**, 2535–2539 (2009)
- Timmins, L.H., Meyer, C.A., Moreno, M.R., Moore, J.E.: Effects of stent design and atherosclerotic plaque composition on arterial wall biomechanics. *J. Endovasc. Ther.* **15**, 643–654 (2008)
- Topoleski, L.D., Salunke, N.V.: Mechanical behavior of calcified plaques: a summary of compression and stress-relaxation experiments. *Z. Kardiol.* **89**, S085–S091 (2000)
- Topoleski, L.D., Salunke, N.V., Humphrey, J.D., Mergner, W.J.: Composition- and history-dependent radial compressive behavior of human atherosclerotic plaque. *J. Biomed. Mater. Res.* **35**, 117–127 (1997)
- Versluis, A., Bank, A.J., Douglas, W.H.: Fatigue and plaque rupture in myocardial infarction. *J. Biomech.* **39**, 339–347 (2006)
- Volokh, K.: Prediction of arterial failure based on a microstructural bi-layer fiber-matrix model with softening. *J. Biomech.* **41**, 447–453 (2008)
- Walraevens, J., Willaert, B., De Win, G., Ranftl, A., De Schutter, J., Vander Sloten, J.: Correlation between compression, tensile and tearing tests on healthy and calcified aortic tissues. *Med. Eng. Phys.* **30**, 1098–1104 (2008)
- Walsh, M.T., Cunnane, E.M., Mulvihill, J.J., Akyildiz, A.C., Gijssen, F.J., Holzapfel, G.A.: Uniaxial tensile testing approaches for characterisation of atherosclerotic plaques. *J. Biomech.* **47**, 793–804 (2014)
- Weisbecker, H., Pierce, D.M., Holzapfel, G.A.: Modeling of damage-induced softening for arterial tissue. In: *Proceedings of the 2011 SCATH Joint Workshop on New Technologies for Computer/robot Assisted Surgery*, Graz, pp. 1–4 (2011)
- Weisbecker, H., Pierce, D.M., Regitnig, P., Holzapfel, G.A.: Layer-specific damage experiments and modeling of human thoracic and abdominal aortas with non-atherosclerotic intimal thickening. *J. Mech. Behav. Biomed. Mater.* **12**, 93–106 (2012)
- Wenk, J.F., Papadopoulos, P., Zohdi, T.I.: Numerical modeling of stress in stenotic arteries with microcalcifications: a micromechanical approximation. *J. Biomech. Eng.* **132**, 091011 (2010)
- Wong, K.K., Thavornpattanapong, P., Cheung, S.C., Sun, Z., Tu, J.: Effect of calcification on the mechanical stability of plaque based on a three-dimensional carotid bifurcation model. *BMC Cardiovasc. Disord.* **12**, 7 (2012). doi:[10.1186/1471-2261-12-7](https://doi.org/10.1186/1471-2261-12-7)
- Zahedmanesh, H., Kelly, D.J., Lally, C.: Simulation of a balloon expandable stent in a realistic coronary artery-determination of the optimum modelling strategy. *J. Biomech.* **43**, 2126–2132 (2010)